TURBULENT DIFFUSION OF SODIUM VAPOR TRAILS

IN THE UPPER ATMOSPHERE

by

Owen R. Coté

A.B. Dartmouth College

(1953)

Submitted in Partial Fulfillment

of the Requirements for the

Degree of Master of

Science

at the

Massachusetts Institute of Technology

June, 1964

Signature of Author . . . .
Department of Meteorology, May 22, 1964

Certified by . . . .

Accepted by . . . .
Chairman, Departmental Committee on Graduate Students

TURBULENT DIFFUSION OF SODIUM VAPOR TRAILS

IN THE UPPER ATMOSPHERE

by

Owen R. Coté

Submitted to the Department of Meteorology on May 22, 1964
in partial fulfillment of the requirements
for the degree of Master of Science

ABSTRACT

The relative dispersion of artificially generated sodium vapor clouds at altitudes between 100 and 117 km is investigated in this study. From sequential photographs the apparent radial expansion is measured both by densitometry and by visual techniques. Interpretation of the apparent expansion of the cloud requires distinction between several optical effects, such as the changing sky background brightness and film sensitivity, and the dispersive effects of the atmosphere, such as turbulent and molecular diffusion.

The variance (relative dispersion) of the radial distribution, which is assumed to be a Gaussian function, is shown to be a linear function of time above 110 km (molecular diffusion). Below 110 km the variance is shown to approximate a t^2 functional form for a morning twilight cloud, and a t^3 form for an evening twilight cloud. Although it cannot be unambiguously demonstrated at this time, the author suggests that the observed t^3 form for the evening twilight case reflects the non-dispersive effect of a decreasing sky background brightness.

The mean square "turbulent" velocity associated with the accelerated cloud growth below 110 km is of the order 2 to 4 m^2/sec^2.

Thesis Supervisor: Norman A. Phillips
Title: Associate Professor of Meteorology

ACKNOWLEDGMENTS

Greatful acknowledgment is made to Professors Norman A. Phillips and Reginald E. Newell for the many helpful discussions of this problem. Their regard for and direction toward simplicity and clarity of expression is, hopefully, at least partially reflected here. Further acknowledgment is made to Dr. Edward Manring and Mr. John Bedinger for access to the sodium trail photographs, and to Messrs. S. Zimmerman and T. Noel who supplied me the data on Cesium clouds used in figures (12) and (13).

The burden of typing the various drafts, as this manuscript evolved, was patiently borne by my wife; that burden is no longer but the "Te Deum" continues. Miss Joy Fanning kindly and artfully executed the drawings.

TABLE OF CONTENTS

List of Figures

List of Tables

I. Introduction

Within recent years various types of rocket experiments have become an increasingly important tool for probing the upper atmosphere. In one such experiment luminous trails of sodium vapor are formed at twilight. The experimental objective of which is a determination of the wind field from the time transport of the cloud axis. The sodium vapor in these trails, when illuminated by solar radiation, emits the characteristic "yellow" D line fluorescence at 5890 and 5896 Å. At twilight, when the sun is depressed from 6 to 9 degrees below the horizon, the cloud at 90 to 120 km is still illuminated by the sun, while the intensity of the diffuse sky background illumination is reduced sufficiently to obtain cloud photographs.

From successive cloud photographs the atmospheric wind field is obtained. Usually the wind field is determined from the first two to three minutes of the photographic sequence, during which time the changes in sky background brightness do not influence the accuracy of the wind determination. Thus, when film was selected and camera stop settings programed, the emphasis was on selecting yellow sensitive film with maximum response to a narrow range of luminous intensity, rather than a lesser response to a broader range of luminous intensity. (For diffusion studies, a flatter response is more advantageous for recording changes of light intensity over the total period in which the cloud is photographed).

The present study will demonstrate that a more precise delineation of film sensitivity is needed to determine the time dependent form of the sodium cloud expansion. Since this precision was not necessary to determine wind profiles, we may expect to find limitations when using the photographic sequences to study cloud expansion. There is, nevertheless, value in analyzing these photographs.

In this study we analyze photographs of sodium vapor trails for evidence concerning the nature of their diffusive growth. Among the questions that must be considered are the following. How is the atomic particle density distribution obtained from photographs which record the distribution and time variation of the cloud luminous intensity? How are the time changes in the width of the luminous trail to be interpreted? Are they due solely to diffusive processes? How do changes in sky background intensity or attenuation effects within the atmosphere affect the apparent growth of the luminous trail? What does the apparent growth of the luminous trail indicate about atmospheric dispersion; is it molecular or turbulent?

II. BACKGROUND TO THE PROBLEM

A. Background to Turbulent Dispersion Theory

Turbulent diffusion is a familiar experience to all who observe stack smoke on windy days or stir cream into their coffee. Despite its common occurence in the physical world very little progress has been made in developing an adequate and complete theoretical description. Turbulent motions are dissipative, dispersive, and characterized by random but continuous velocity fluctuations. The unpredictability of the random turbulent velocity forces the sacrifice of detailed understanding of the motion to descriptions by probability density functions (p.d.f.). The p.d.f. may be obtained by theoretical arguments or, empirically, from a large number of reproducible experimental trials.

Consider the case of two particles released into a turbulent fluid. The ensemble of such experiments will generate the joint probability distribution function $Q(\underline{x}', t'; \underline{x}'', t'' | \underline{x}'_o, t'_o; \underline{x}''_o, t''_o)$. This is the probability that particles which originated at $\underline{x}'_o$ and $\underline{x}''_o$ at t'_o and t''_o, respectively, will have travelled to $\underline{x}'$ and $\underline{x}''$ at t' and t''. By replacing $\underline{x}'$ and $\underline{x}''$ by $\underline{X} = \underline{x}' - \underline{x}'_o$ and $\underline{y} = \underline{x}'' - \underline{x}'$, we may distinguish the translation of the particle pair from their separation. If we consider only the relative displacement, $\underline{y}$, of the two particles at $\underline{x}'$ and $\underline{x}''$ then the function of interest becomes

$$Q(\underline{y}, t | \underline{y}_o, t_o) = \int Q(\underline{y}; X, t | \underline{y}_o; X_o, t_o)\, dX \qquad (2.1)$$

where $Q(\underline{y}, t | \underline{y}_o, t_o)$ is called the separation p.d.f.

For dispersion studies the most meaningful parameter derivable from the separation p.d.f. is its second integral moment, which we call the relative dispersion tensor. A typical element of this tensor is designated σ_{ij} ($i = 1, 2, 3$; $j = 1, 2, 3$)

$$\sigma_{ij}\ (t|\underline{y}_o, t_o) = \langle y_i(t)\, y_j(t) \rangle = \int y_i y_j\, Q(\underline{y}, t|\underline{y}_o, t_o)\, dy \qquad (2.2)$$

The symbol, $\langle\ \rangle$, represents an ensemble average. Furthermore, the relative dispersion may be related to the relative velocity of the two particles as follows

$$\langle y_i(t)\, y_j(t) \rangle = \Big\langle y_i(t_o)\, y_j(t_o) \Big\rangle + \int_{t_o}^{t} dt' \int dt'' \langle v_i(t')\, v_j(t'') \rangle \qquad (2.3)$$

The one-dimensional form of the relative dispersion, σ^2, follows from (2.2)

$$\sigma^2\ (t|y_o, t_o) = \Big\langle y^2(t) \Big\rangle = \int y^2\, Q\,(y, t|y_o, t_o)\, dy \qquad (2.4)$$

The "shape" of a luminous sodium cloud is directly related to the possibility of a vector $\underline{y}$ being completely immersed in the cloud. As Batchelor (1952) has shown, once the initial shape of a luminous cloud is known, its subsequent tendency to change will be determined by the statistical properties of the separation of two "particles", i.e. the separation p.d.f. Specific predictions of cloud growth in the form

$$\sigma^2 = \langle r^2 \rangle \sim t^{\alpha}$$

where α is one, two, or three may be obtained from the various theoretical formulations of turbulent diffusion theory discussed in the next section.

B. Theoretical Predictions of Turbulent Dispersion

The most widely known theory of turbulent diffusion is Kolmogorov's similarity or universal equilibrium theory (See Batchelor, 1950). The similarity theory develops from the idea that some kind of statistical decoupling accompanies the transfer of energy from the large scale to the small scale motions where the small eddies tend to be statistically isotropic. The theory is formulated into two similarity hypotheses:

(1) "The statistical properties of the small-scale components of any turbulent motion with large Reynolds numbers are determined uniquely by the quantities η and ϵ " (kinematic viscosity and turbulent energy dissipation).

(2) "At sufficiently large Reynolds numbers of the turbulence, there is an inertial subrange in which the average properties are determined uniquely by the quantity ϵ " (Batchelor, 1950).

One can associate a characteristic length l_o with a range of wave numbers in which most of the energy is contained, and a characteristic rms speed, $u_o = 1/3 < u_j u_j >^{\frac{1}{2}}$. If the initial separation vector, $\underset{\sim}{y}_o$, is small in comparison with the length scale, l_o, then the universal equilibrium theory may be assumed valid. The relative dispersion, $< \underset{\sim}{y}^2 >$, is expressed as a universal function of the parameters, η and ϵ, describing the turbulence, and the variables, t and y_o. Batchelor (1950, 1952) gives the following predictions as a consequence of the similarity theory:
At small values of time, $t \ll y_o^{2/3} \epsilon^{-1/3}$

$$< \underset{\sim}{y}^2 > - < \underset{\sim}{y}_o^2 > \sim t^2 (\epsilon y_o)^{2/3} \qquad (2.5)$$

at intermediate values of time, $t \gg y_o^{2/3} \epsilon^{-1/3}$ (provided y is still within the limits of the inertial range)

$$\langle y^2 \rangle \sim \epsilon t^3 \qquad (2.6)$$

A similar prediction results from a recent theory of Lin (1960), in which he assumes that the forces acting on the dispersing particles may be described by a stationary random anisotropic process, but the relative velocity covariance (of two particle separtion) may not. The final form of this theory is an asymptotic result for diffusion times within a certain time interval $\tau_1 < t < \tau_2$. The time, τ_1, is determined by the acceleration covariance becoming negligibly small. The time, τ_2, although greater than τ_1, is still small enough so that the relative velocity autocorrelation is not independent of diffusion time. The final prediction takes the form

$$\langle y^2 \rangle = 2/3\ \tilde{B} t^3 \qquad (2.7)$$

This form of the relative dispersion (mean square separation) is similar to the similarity prediction (2.6). Although $\tilde{B}$ and ϵ are dimensionally the same they are not necessarily equal (Lin proposes, without proof, that $\tilde{B}/\epsilon$ is equal to a universal function of the Reynolds number). Furthermore, Lin's result does not require the assumption of local isotropy.

One other theory deserves brief mention. It was proposed by C. M. Tchen (1954, 1961). From predictions for the energy spectrum function and the shear spectrum function in the inertial subrange (Fourier wave number space), Tchen derives relative diffusion laws for large and small values of mean flow shear. When the mean flow shear is large, the prediction of relative dispersion is

$$< y^2 > \sim t^2 \qquad (2.8)$$

and when the mean flow shear is small, the prediction is similar to (2.6) and (2.7)

$$< y^2 > \sim t^3 \qquad (2.9)$$

(the factors which would change the proportionality in (2.9) to an equality are unspecified by Tchen).

A final example of the prediction of a t^2 regime for relative dispersion follows from a simple model developed by Kraichnan (1962). Consider the three dimensional problem where the velocity field $u_i(x)$ has an isotropic, multivariate normal distribution, which is independent of time in each realization, and the concentration φ satisfies the equation

$$\frac{\partial \varphi}{\partial t} + u_i \frac{\partial \varphi}{\partial x_i} = K \nabla^2 \varphi \qquad (2.10)$$

where K is the molecular diffusity. The initial mean concentration is given as the three-dimensional Dirac function and the problem reduces to finding the mean concentration

$$P(\underline{x}, t | \underline{x}_o, t_o) = < \varphi (\underline{x}, t) > \qquad (2.11)$$

Kraichnan then distinguishes two asymptotic ranges in which $P(\underline{x}, t|\underline{x}_o, t_o)$ has a simple form. They are $t \ll \ell_o/v_o$ and $t \gg \ell_o/v_o$ where ℓ_o and v_o are the correlation length and root-mean-square speed associated with $u_i(\underline{x})$. The two independent Gaussian processes, molecular diffusion and a Gaussian distributed displacement $t\,u_1(0)$ determine the distribution so that

$$P(\underline{x},\ t|0,0) = 4\pi(Kt + \tfrac{1}{2} v_o^2 t^2)^{-3/2} \exp\left[- \frac{|\underline{x}|^2}{4Kt + 2v_o^2 t^2}\right] (t \ll \ell_o/v_o) \qquad (2.12)$$

and

$$< x_1^2 > = \int x_1^2\, P(\underline{x},\ t|0,0)\, d\underline{x} = 2Kt + v_o^2 t^2 \qquad (2.13)$$

where $< x_1^2 >$ is the mean square displacement in one direction. The effect of molecular diffusion is related to the ratio $\ell_o v_o/K$. For $\ell_o v_o/K \gg 1$ molecular diffusion is negligible except for very short times $t \ll K/v_o^2$.

If the relative dispersion of the sodium cloud with an assumed Gaussian distribution of line-of-sight concentration were given by

$$< r^2 > = \int r^2\, Q(r,t|0,0)\, dr = 2Kt + 2/3\ \tilde{B}t^3 \qquad (2.14)$$

then, physically, this would again imply two independent Gaussian displacements that are mean square additive (Taylor (1935) was the first to suggest this as a useful assumption, and Townsend (1954) has since shown that its closest approximation to experimental result occurs for small diffusion time). The relation $< r^2 > = 2Kt + 2/3\ \tilde{B}t^3$ implies that the velocity is not constant for an independent turbulent displacement, ut, as in (2.12), but is a function of $t^{\frac{1}{2}}$. Dimensionally this implies that $U \sim \sqrt{\tilde{B}t}$, where $\tilde{B}$ is dimensionally equivalent to ϵ of the Kolmogorov similarity theory.

The dispersive influence of the atmosphere upon the cloud will be indicated by the functional form of the time dependence of the variance σ^2 derived from the observed cloud expansion. The quantitative problem of sodium vapor trail expansion is to determine the functional form of the variance associated with the assumed Gaussian distribution of the sodium density.

C. Cloud Photography

An understanding of photographic image formation is necessary to interpret the measurements of sodium cloud expansion. Recording the sodium cloud image requires the proper choice of camera optics and adjustments: focal length of lens, camera aperture opening, exposure time, and film and filter combination.

The various combinations of these elements proper to sodium cloud intensities is discussed in detail by Manring and Levy (1961). In this section a brief review is presented to emphasize the care that must be taken in relating changes in luminous intensity recorded on a film to the diffusive changes in concentrations of light scattering atoms.

The intensity of radiation coming from the cloud is defined as follows. Consider any differential element of area, dA, of any surface in the volume of space. This surface may or may not correspond with the actual physical surface of the cloud. The radiation in the frequency range ν to $\nu + d\nu$, passing per unit time through dA, and confined within the truncated cone defined by dA, and the solid angle, $d\omega$, is denoted by $d\,E_\nu$(erg/sec). The specific intensity, I_ν, is energy per unit frequency interval, transported across unit area perpendicular to the direction of the beam (in direction (ξ, ψ), where ξ is a co-latitude or zenith angle and ψ is an azimuthal angle) in a unit solid angle per unit time;

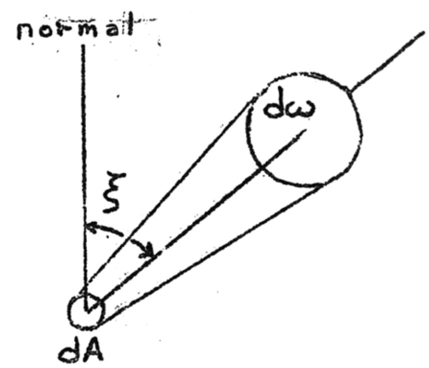

it is expressed symbolically

$$dE_\nu = I_\nu \cos \zeta \, d A \, d\nu \, d \omega$$

The <u>integrated</u> <u>intensity</u>, $\mathcal{I}$, is

$$\mathcal{I} = \int_0^\infty I_\nu d\nu \qquad (2.15)$$

where the units of $\mathcal{I}$ are erg/cm^2 sec sterad. When the unit area in the definition of the integrated intensity also corresponds with the surface of an emitting source, such as a sodium cloud, the <u>surface</u> <u>brightness</u> B of the cloud is defined by $4\pi\mathcal{I}$ where the units are erg/cm^2 sec. (Surface brightness is sometimes expressed in units of photon/cm^2 sec or rayleighs. One rayleigh is 10^6 photon/cm^2 sec; one photon (at λ5893Å) is 3.37 x 10^{-12} erg.)

The relation between the surface brightness, B, at the cloud and the energy received by a recording device, such as a camera, is illustrated in the following manner. The solar illuminated sodium cloud is located at a line-of-sight distance, s, from a camera. If the camera has a lens aperture area, A, then this area subtends a solid angle $\frac{A}{s^2}$ steradian at a point on the cloud surface. The total number of photons emitted from the cloud into this solid angle is $\frac{\mathcal{I}A}{s^2}$.

The total energy, E, received at a point on the camera film plate from a point on the cloud surface during an exposure of t seconds is represented by

$$E \sim \frac{\tau \mathcal{I} A t}{s^2} = \frac{\tau B A t}{4\pi s^2} \qquad (2.16)$$

where τ is the total attenuation between cloud and film. Among the attenuation factors that reduce the total energy received at the camera plate are the transmission of the camera lens system, the filter transmission, and atmosphere transmission effects such as scattering, both Rayleigh and Mie, absorption by the Chappuis bands of ozone (4400 to 7400 Å), and absorption by the natural sodium layer at a height of about 80 km. The logarithmic relation between cloud surface brightness and energy received at the film is expressed

$$\ln E = \ln B - \chi \tag{2.17}$$

where the attenuation and other factors are included in the χ term.

The total intensity of energy per square centimeter incident upon the film determines the degree of darkening of the film negative. This darkening is called the film density, D. The law of darkening for each film is represented by empirical curves of D vs ln E such as those in figure 1 taken from Manring and Levy (1961). (Note that log E in figure 1 is to the base 10.) If the "gamma" of a film is defined by the relation

$$\gamma = \frac{dD}{d \ln E} \tag{2.18}$$

then there are regions of the D vs ln E curve for which γ has a constant (and maximum) value for a finite range of ln E values. The region of constant γ is also the region of sharpest film darkening for a given change in ln E. Energy values to either side of the constant gamma region give darkest film densities on the shoulder of the D vs ln E curve and lightest densities on the toe. In both the toe and shoulder regions there is very small contrast for a finite change in energy received by the film.

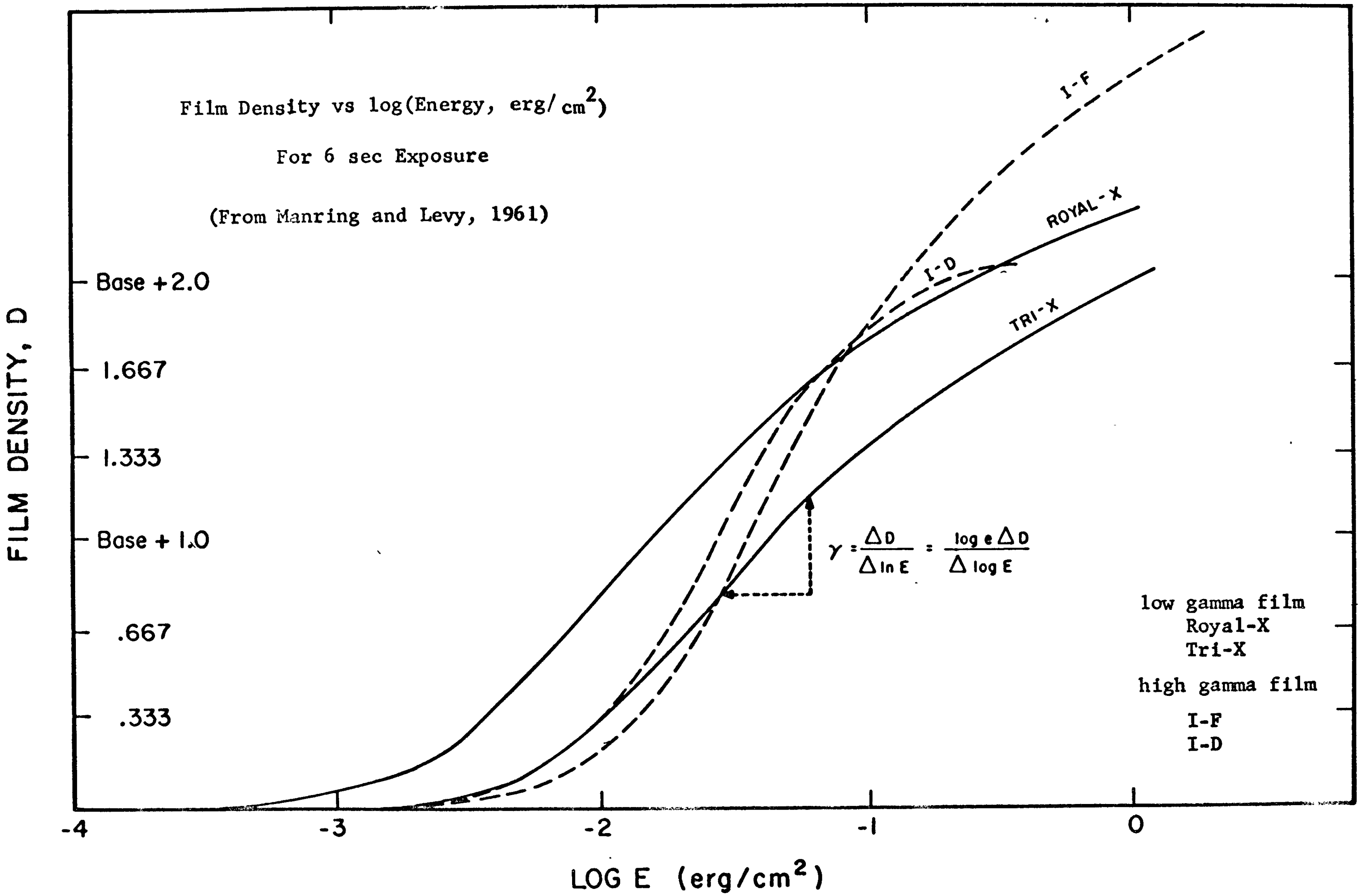

Fig.1. Illustrations of the empirical relationship between the energy received by a film and its degree of darkening, the film density, D.

We now may summarize the relationship between the cloud image as represented by the film density, D, and the atomic sodium number density, ρ, in the cloud (atoms per cc.). The integration of the number density of solar-illuminated sodium atoms over the line-of-sight distance, s, is called the "column density", n, where

$$n = \int_0^\infty \rho\,(s)\,ds \qquad \text{(atoms per cm}^2\text{)} \qquad (2.19)$$

For an optically thin cloud, the surface brightness, B, is proportional to n. If this is expressed

$$B = qn \qquad (\text{erg/cm}^2\text{-sec}) \qquad (2.20)$$

where q has the dimensions erg/atom-sec, then from (2.16), (2.17), and (2.18) it follows that

$$\frac{dD}{\gamma} = d(\ln E) = d\ \ln\,(B\ e^{-K}) = d\ \ln\,(q\ n\ e^{-K}) \qquad (2.21)$$

A simpler relation follows if we consider the relative magnitudes of n, D, and E at different radial distances from the cloud axis (for a fixed time). If n, D, and E represent the respective qualities at a distance r from the cloud axis, and n_o, E_o, and D_o represent the same quantities along the cloud axis, then for an optically thin cloud (2.21) may be expressed

$$\frac{D - D_o}{\gamma} = \ln E/E_o = \ln n/n_o \qquad (2.22)$$

(2.22) is valid if the range of energy E associated with the sodium cloud remains within the region where γ is a constant. To help accomplish this, filters are chosen with a cutoff to the short wave side of 5893Å and films are chosen which are relatively insensitive to the long wave side of 5893Å. Thus the film-filter combination is chosen to maximize sensitivity to intensity near 5893Å and minimize sensitivity to intensity coming from the sky background at other wave lengths.

III. METHODS OF CLOUD GROWTH MEASUREMENT AND ANALYSIS

A. Introduction

The observational data available for this study are sequences of photographic negatives from five camera sites. Three film and lens combinations are used: 80 mm f/2.8 lens with 70 mm roll film, and a K-24 aerial camera using 5" x 7" strip film with either 7" f/2.5 or 20" f/5.6 lens. Exposure times used with the 70 mm film were 3, 6, and 12 seconds.

An example of the Wallops Island photographs used in this study is given in figure 2. These photographs show wind distorted clouds whose surface appearance runs from faint and irregular to bright and smooth. This gradual evolution into a smooth trail characterizes, to my knowledge, all sodium clouds. One might characterize the stages as "irregular", "globular", and "smooth." The globular region is particularly well pronounced in the 17 September cloud in 2b. Whether these irregularities in appearance are due to atmospheric turbulence, or to an irregular deposition during the ejection process (the irregularities are progressively obscured by the increasing rate of molecular diffusion at higher levels) is not known. But, as we shall show later, accelerated cloud expansion may occur in the smooth regions below 110 km.

Figure 3 indicates the relative location of the five camera sites. In order to compute cloud height and position, images from five simultaneous photographs are projected onto a hemispheric dome, each projector being located and oriented as the camera which it models. The intersection of taut

(a) 9 December 1960 (AM)

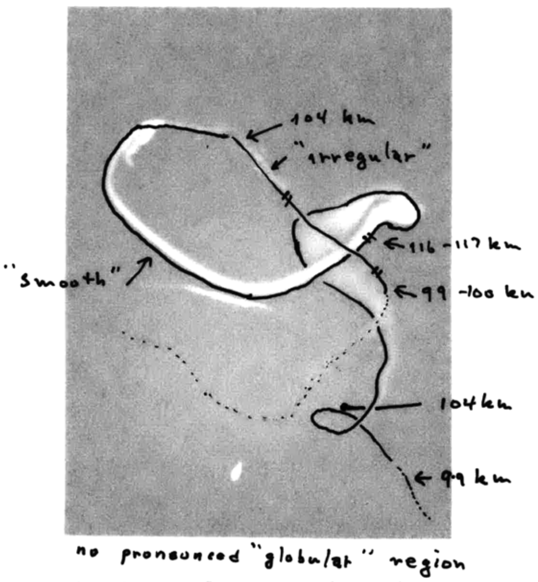

6 min. after rocket launch

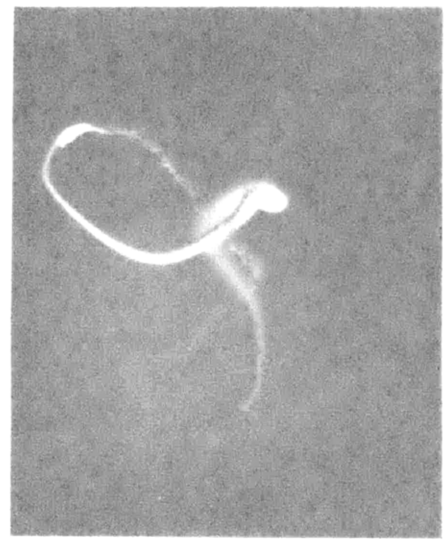

5 min. after rocket launch

Note that the straight region just before loop in the up trail cloud is irregular and the corresponding parallel straight region in down trail is smooth.

(b) 17 September 1961 (AM)

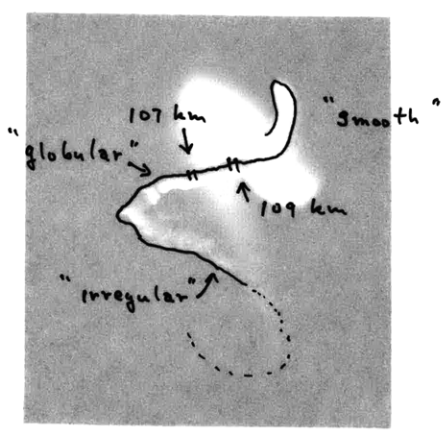

6 min. after rocket launch

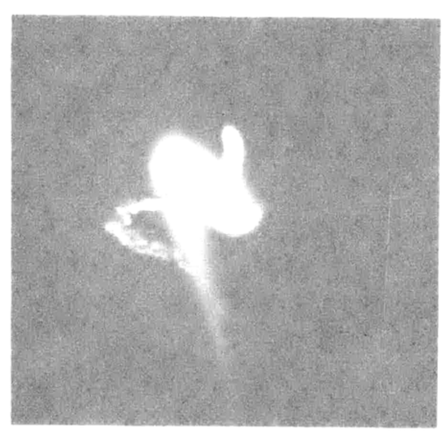

5 min. after rocket launch

Fig. 2. View of clouds from Wallops Island rocket launch site (F-24 7" f/2.5 data)

(a) 9 December 1960 (AM)

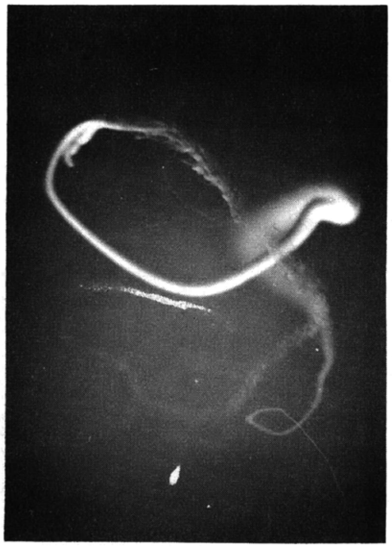

6 min. after rocket launch

5 min. after rocket launch

Note that the straight region just before loop in the up trail cloud is irregular and the corresponding parallel straight region in down trail is smooth.

(b) 17 September 1961 (AM)

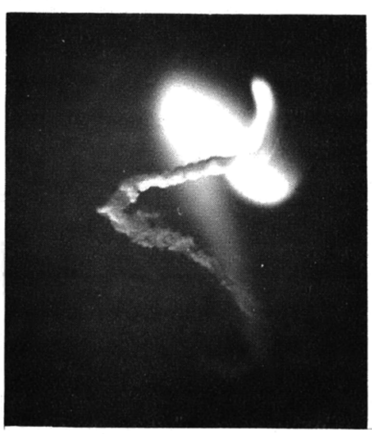

6 min. after rocket launch

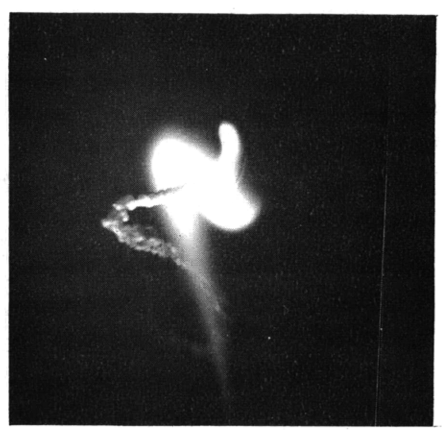

5 min. after rocket launch

Fig. 2. View of clouds from Wallops Island rocket launch site (K-24 7" f/2.5 data)

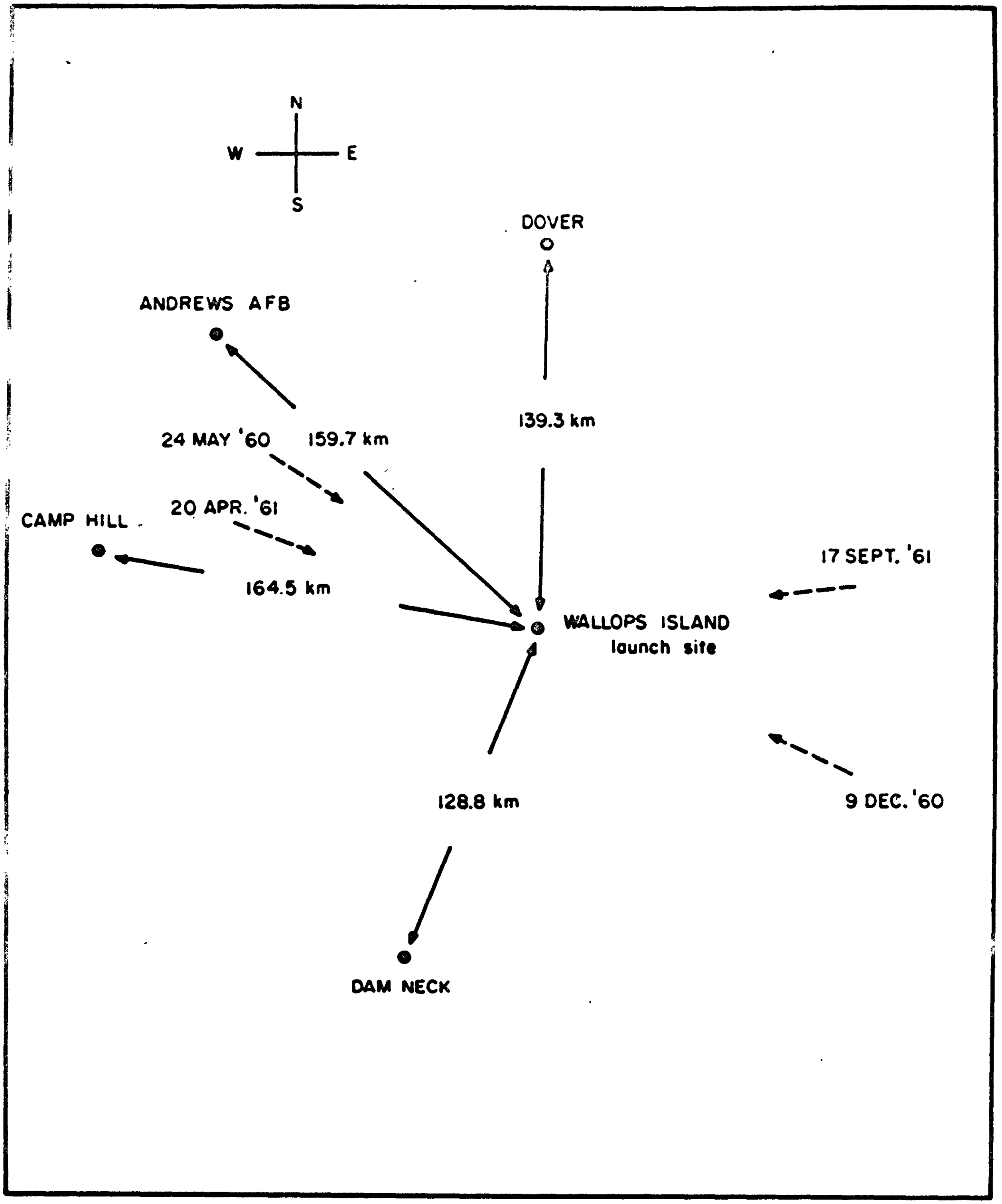

Fig. 3. Relative position of camera sites to the Wallops Island Launch Site. Dashed arrows represent the solar azimuth angle of the sun at 7° solar depression during cloud photography of four specific sodium trails.

nylon strings running from each projector to its respective cloud image determines the spatial position of "points" in the cloud. The measured cloud coordinates in the model geometry are converted to actual heights and distances by appropriate scaling factors.

B. Measurement Techniques

Diameter measurements are obtained by two methods. In the "microscope" method we use a small microscope mounted on a lead screw with one dimensional motion and calibrated to .01 mm (obtained from the David Mann Company, Concord, Massachusetts). This device is capable of measuring a well defined cloud edge to 0.02 mm. This represents about 30 to 40 meters at the typical cloud range from the outlying camera sites. For late diffusion times the luminosity gradients are smaller and the accuracy of microscope measurements deteriorated rapidly. More objective measurements of cloud diameters are then obtained by densitometry across a cloud diameter. In addition to the diameter of the cloud, a distribution of film density D with distance across the diameter is obtained. In all densitometer measurements an attempt is made to duplicate the measurements of the "microscope" method. The diameter of the cloud on the negative (in mm) is converted to actual cloud diameter (in km) by multiplying by the ratio of the range (km) to the focal length of the lens (mm).

Measurements of cloud diameters are made in the irregular part of the cloud for 9 December 1960 (A.M.) and 20 April 1961 (P.M.). They are made in the "globular" region, or just above, on 17 September 1961 (A.M.) and 24 May 1960 (P.M.). The heights at which these measurements are made varied from 99 to 109 km. On films illustrated in figure 2a for 9 December, measurements are also made well up in the smooth part of the trail at 116 to 117 km. The crossmarks on the overlay to figure 2 indicate locations where cloud diameter was measured or densitometer traces obtained. Measurements of cloud diameters in the 20 April 1961 (P.M.) photographs are made between 100 and 104 km, and are indicated by the portion of trail between "a" and "b" in figure 4.

Cloud diameter measurements cannot be made at every height on a cloud photograph. The reason for this is illustrated by the trail image marked "c" in figure 4. The direction of cloud transport in the plane of the photograph is marked by the arrow in figure 4 and, as can be seen, is essentially perpendicular to the trail axis or parallel to the cloud diameter. The amount of cloud tran port in the six second exposure time for the film contributes a spurious thickness to the trail diameter at "c". With a transport of 50 m/sec perpendicular to the direction of the camera line-of-sight, the cloud is transported 300 meters during a six second exposure. The film integrates the intensity emitted by the cloud and a significant error will result in measured cloud diameters when the actual cloud diameter is 1 or 2 km or less.

The motion of cloud material at "a" and "b" in figure 4 is essentially along the trail axis. This stretches the cloud along the line "a" to "b" but the motion does not contribute to the image of the cloud diameter. A similar effect of motion on cloud image occurs in photographs from the outlying camera sites. On the negatives for these sites, diameter measurements (or densitometry) are only made across diameters at those heights where the wind transports the cloud in a direction toward or away from the recording camera.

Fig. 4. View of cloud on 20 April 1961 (P.M.) from Wallops Island launch site (K-24 7" f/2.5)

C. Analysis Techniques

A measured sodium cloud diameter on a film negative represents the distance between certain equivalent intensity levels of the sodium fluorescence. As long as the surface brightness received by the film is proportional to the number of atoms/cm^2 along a line-of-sight, something can be learned about the diffusion of sodium atoms by following an isophote expansion in time. Care must be maintained that conclusions about diffusion of sodium clouds are always based upon isophote changes caused by sodium density changes.

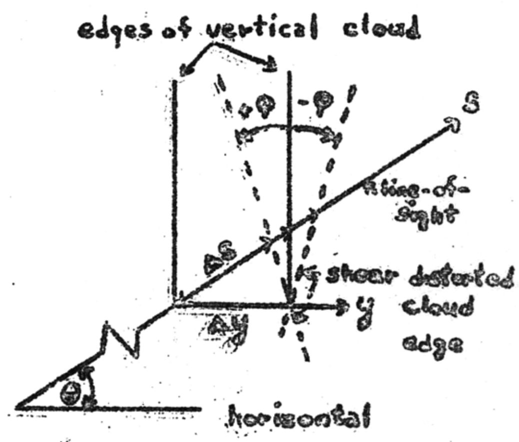

θ = elevation angle

$\varphi = \arctan\left|\dfrac{\Delta v_s}{\Delta z}\Delta t\right|$

$\mu = \cos\theta + \sin\theta\tan(\pm\varphi)$

For an approximately cylindrical cloud, whose central axis is initially vertical, the line-of-sight distance through the cloud, Δs, will be related to the horizontal thickness of the cloud, Δy, by $\Delta s = \dfrac{\Delta y}{\cos\theta}$ where θ is the elevation angle of the camera. Vertical shear of line-of-sight wind component, V_s, will cause a rotation of the cloud axis. The resulting relation between line-of-sight through the cloud, and the horizontal thickness of the cloud, is expressed $\Delta s = \dfrac{\Delta y}{\mu}$, where μ is a geometrical factor which includes the effects of wind shear in addition to the zenith angle of observation (see figure insert). For a cylindrical cloud in which the horizontal distribution of atomic sodium is a Gaussian function, the number of atoms per square centimeter column, n, is

$$n(r,t) = \frac{N}{\mu(2\pi\sigma^2)^{\frac{1}{2}}}\exp\left[-\frac{r^2}{2\sigma^2}\right] \qquad (3.1)$$

where

n is the number of sodium atoms per square centimeter line-of-sight column (atom/cm^2);

N is the linear density of atomic sodium deposited in the atmosphere by the rocket (atom/cm);

r is the horizontal radial distance from cloud axis in a plane perpendicular to the line-of-sight;

σ^2 is the time dependent variance of the Gaussian function n;

μ is a geometrical factor determined by wind shear and elevation angle of observation.

As long as n is less than 10^{11} atom/cm^2 the cloud is optically thin and the surface brightness of the luminous cloud is proportional to n (Donahue and Foderaro, 1955). At some distance from the central axis of the cloud there is a value of n at which the surface brightness of the cloud is just distinguished from the sky background surface brightness (either visually or by densitometry). This value n_e defines the <u>visual diameter</u>, D_e, of the cloud ($r_e = \frac{D_e}{2}$).

The distribution of darkening in a photographic image of the cloud can be related to the number of sodium atoms per square centimeter column, when the cloud is optically thin and the film sensitivity is known. The mean square dispersion of the sodium vapor (the variance, σ^2, of the Gaussian distribution of n) can then be computed directly from cloud photographs. To estimate the quantitative nature of the diffusivity of the upper atmosphere, the time rate of change of the variance, σ^2, must be determined. In what follows, we derive three different methods for obtaining σ^2 from cloud photographs. For brevity, we call the methods: the central intensity, the gradient log column density, and the maximum radius.

a) Central intensity method

At the cloud axis ($r = 0$) the column density, n_o , for a particular height, is given by (3.1)

$$n_o (t) = \frac{N}{\mu (2\pi\sigma^2(t))^{\frac{1}{2}}} \qquad (3.2)$$

If μ does not change and there are no sources or sinks to change the value of N, the ratio of n_o at t and a later time $t + \Delta t$ is

$$\frac{n_o (t)}{n_o (t + \Delta t)} = \sqrt{\frac{\sigma^2 (t + \Delta t)}{\sigma^2 (t)}} \qquad (3.3)$$

If γ and K are both constant, then it follows from (2.21) that (at a fixed radius).

$$\frac{D_o (t + \Delta t) - D_o (t)}{\gamma} = \ln\left(\frac{n_o (t + \Delta t)}{n_o (t)}\right) \qquad (3.4)$$

Substituting (3.3) into (3.4) gives

$$\frac{D_o (t) - D (t + \Delta t)}{\gamma} = \frac{1}{2} \ln\left(\frac{\sigma^2 (t + \Delta t)}{\sigma^2 (t)}\right) \qquad (3.5)$$

From this last relation, σ^2 may be computed from successive cloud photographs, if σ^2 is known at any one time, say, at $t = 0$.

The requirements for using this method are most likely to be found in small spherical puffs of alkali metal vapor and not in the more optically dense sodium trails. For example, the usual sodium payload is 2kg or approximately 87 moles; the total number of sodium atoms is about 5×10^{25} atoms. The linear density (atom/cm) of sodium atoms ejected along the rocket trajectory is not known exactly, but a rough estimate is possible. If the sodium ejection is uniform over the three minutes of vaporizer burning time, about 3×10^{23} atom/sec can be released into the atmosphere. Radar tracking indicates the upward speed of the rocket averages about 1000 meters/sec at 100 to 117 km; in 10^{-5} second the rocket moves 1 cm. Linear densities (atom/cm) up to 2×10^{18} atoms/cm are generated if the vaporization process is 100% efficient. A more reasonable efficiency may be closer to 5% (Marmo et al 1960). Thus, N is estimated to be 10^{17} to 10^{18} atoms/cm.

The initial visual diameter of the sodium cloud, about one second after rocket passage, is estimated from photographs to be about 100 meters. For a Gaussian distribution the initial variance σ_o can be computed (see equation 4.2) for reasonable assumptions about the column density at $r_e = 50$m. If the range of n_e is 5×10^9 to 10^{10} atoms/cm^2 (Chamberlain, 1961), and N ranges from 10^{17} to 10^{18} atoms/cm, the σ_o value ranges from 21.8 to 23.5 meters. For the values, $\sigma_o = 22$ meters and $N = 5 \times 10^{17}$ atom/cm, the initial column density through the trail axis ($r = 0$) is approximately 10^{14} atom/cm^2. This indicates an optical thickness of 10^3 if $\tau = 1$ is equivalent to $n = 10^{11}$ atom/cm^2. Thus, the surface brightness of the cloud at $r = 0$ is not proportional to the column density and the central intensity method is not applicable. This method has not been used in this study.

b) The maximum radius method

In this method we assume the visual edge of the cloud corresponds with the same isophote at all times. In terms of the surface density, n, the assumption implies that the darkening of the film negative by the sky background neither increases nor decreases in time. Thus the visual edge of the cloud is defined at all times by a constant value of n, n_e. From (3.2), $\mu = 1$, and $\frac{dn_e}{dt} = 0$ it follows that

$$\frac{d\, r_e^2}{d\, t} = \frac{d\, \sigma^2}{d\, t} \left(\frac{r_e^2}{\sigma^2} - 1 \right) \qquad (3.6)$$

Since $\frac{d\sigma^2}{dt}$ is positive by definition (the mean square dispersion increases with time), the expansion of the isophote defined by r_e ends when $r_e^2 = \sigma^2$, while at the same time, equation (3.2) reduces to

$$\frac{n_e}{N} = \frac{1}{\sqrt{2\pi e r_e^2}} = \frac{1}{\sqrt{2\pi e r^2}} \qquad (3.7)$$

Furthermore, since $\frac{dn_e}{dt} = 0$, $\frac{n_e}{N}$ is a constant which may be eliminated from (3.2) and (3.7). If we let $\rho^2 = r_e^2$ (max) the resulting equation is

$$\sigma^2 = r_e^2 \left\{ \ln (\rho^2 e) - \sigma^2 \right\}^{-1} \qquad (3.8)$$

This transcendental equation in σ^2, ρ^2 and r_e^2 may be used to compute σ^2 for any measured r_e^2 provided ρ^2 is also known.

The utility of this method is affected by the changing surface brightness of the sky. During the period of cloud photography the solar depression angle varies from about 6 to 9 degrees. The relative zenith brightness of the night sky may be inferred from a study by Korchignia et. al. (1959) who have measured the relative zenith brightness between 3300Å and 5000Å from night through day. Their results are plotted in figure 5 as a function of solar depression angle. It should be noted from figure 5 that the zenith brightness changes by about two orders of magnitude during the period of sodium cloud photography. A change in brightness of this magnitude is equivalent or greater than the range of ln E (in figure 1) for which γ is effectively constant. Thus, the changing surface brightness of the night sky is seen to be an important consideration in the interpretation of cloud photographs.

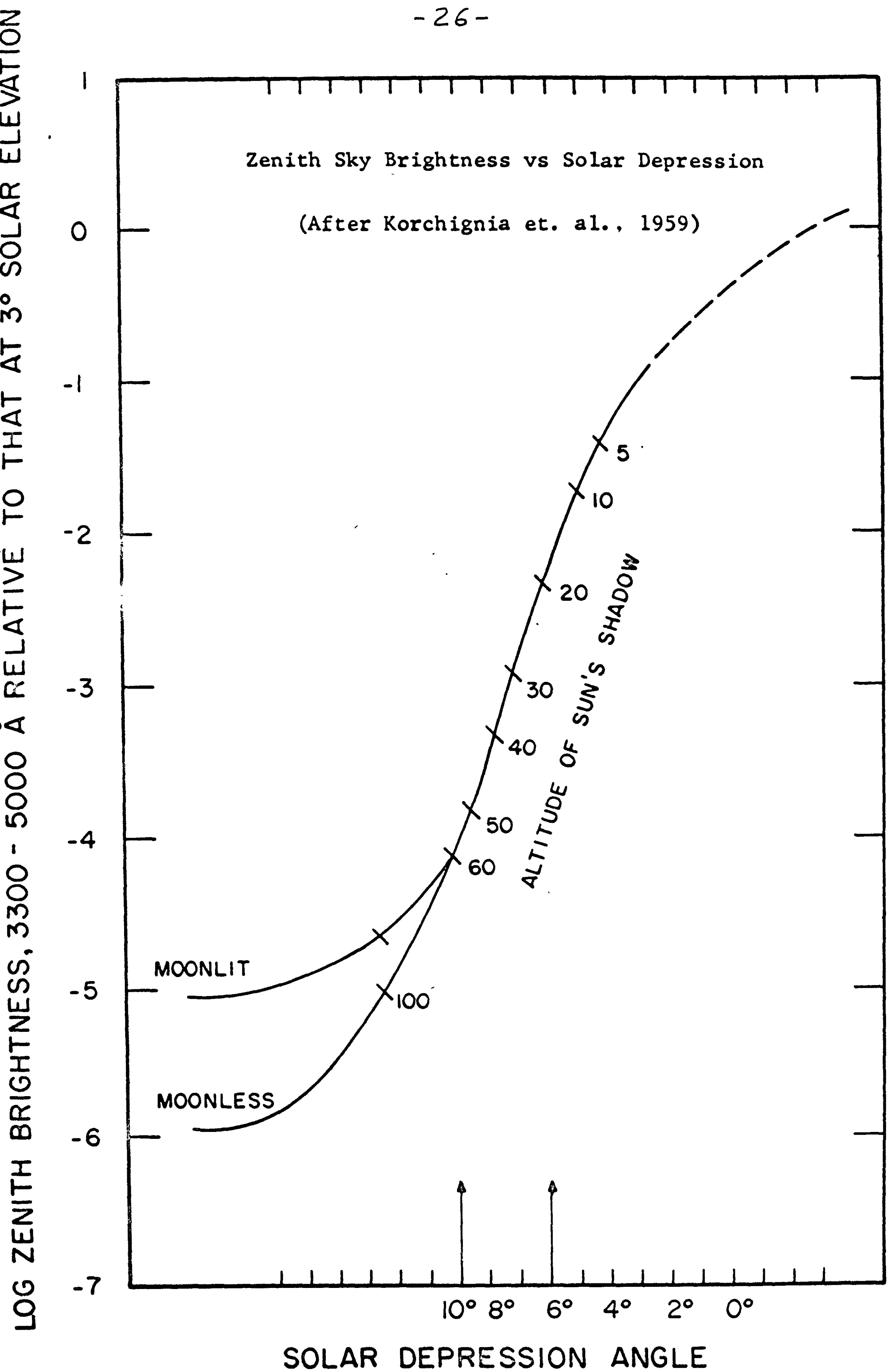

Fig. 5. Typical variation of Zenith Sky Brightness at 4000 Å with changes in solar depression angle.

c) Gradient log column density method

For a Gaussian distribution of sodium vapor the rate of change of n with radial distance from the cloud axis (at a given time, and therefore, fixed σ^2) may be expressed

$$\frac{\partial n}{\partial r} = - \frac{r}{\sigma^2} \frac{N}{(2\pi\sigma^2)^{\frac{1}{2}}} \exp\left[- \frac{r^2}{2\sigma^2} \right] = - \frac{rn}{\sigma^2}$$

so that

$$\sigma^2 = -\frac{1}{2} \frac{\partial r^2}{\partial \ln n} = \frac{1}{2} \frac{r_2^{\,2} - r_1^{\,2}}{\ln \frac{n1}{n2}} \qquad (3.9)$$

The profile of film density, D, against radius, r, is obtained from densitometer traces. When $\frac{dD}{d \ln E}$ is a constant it can be expressed

$$\frac{D_2 - D_1}{\gamma} = \ln (E_2/E_1)$$

If we neglect any variation in absorption cross-section and incident solar flux between the line-of-sight through the cloud at radius r_1, and r_2, then for column denstities, n, less than 10^{11} atom/cm^2 ln E is proportional to ln n

$$\ln (E_2/E_1) = \ln (B_2/B_1) = \ln (n_2/n_1)$$

The variance may then be obtained from the difference in film density at these two radii in the form

$$\sigma^2 = - \frac{\gamma}{2} \frac{r_2^{\,2} - r_1^{\,2}}{D_2 - D_1} \qquad (3.10)$$

where r_1 is greater than or equal to the radius where the surface density is 10^{11} atom/cm^2.

With this method the variance may be computed for a given photograph from the distribution of film density (for a particular height). Changes in sky background will not influence the magnitude of the computed σ^2 value in (3.10) (if γ remains constant). In a morning twilight it will, however, contract the range, Δr^2, between r_e^2 and r_1^2 (if in (3.10) we associate r_1^2 with an n equal to 10^{11} atom/cm^2) for clouds on successively later negatives.

Approximations to the gradient ln (n) method are used by Manring et al (1961) and Blamont and Baguette (1961) to compute molecular diffusion coefficients. In addition to making most of their measurements above 104 km, where the trails are usually smooth, they also assume that σ^2 in (3.10) has the form $\sigma^2 = 2$ Kt for cylindrical trails, and $\sigma^2 = 4$ Kt for spherical puffs.

As a first approximation to σ^2, Blamont and Baguette chose the radius, r_2, where the film density is .368 or (1/e) of the cloud axis film density, D_o. They compute values of K from the slope of r_2^2 vs t. In terms of (3.10) this may be expressed

$$\sigma^2 = - \frac{\gamma}{2} \frac{(r_2^2 - o)}{\frac{D_o}{e} - D_o} = r_2^2 \frac{\gamma}{1.26\ D_o} \qquad (3.11)$$

so that $\sigma^2 \cong r_2^2$ implies $\frac{\gamma}{D_o} \cong 1.26$ or $\gamma \cong 1.26\ D_o$. Thus, th[illegible]chnique used by Blamont and Baguette is exactly equivalent to the gra[illegible]t ln (n) method, if γ and the film density at the center of the cloud image satisfy the relation, $\gamma \cong 1.26\ D_o$. Since the film used by Blamont and Baguette is TRI-X with a γ of about 0.4 (see figure 1), this suggests that Blamont's diffusion coefficients will be greater than those computed with the exact formula when $D_o > 0.3$ and less when $D_o < 0.3$. Our measurements of the maximum film density of sodium clouds on TRI-X negatives would suggest that Blamont and Baguette's diffusion coeficients can be a factor of three or four larger than the value obtained with the exact formula (with $\gamma \sim 0.4$).

In Manring's technique for computing molecular diffusion coefficients another approximation to (3.10) is used. He computes diffusion coefficients, K from the formula

$$K = \frac{\sigma^2}{4t} = \frac{r_2^{\ 2} - r_1^{\ 2}}{4t \ \ln \frac{\tilde{E}_1}{\tilde{E}_2}} \qquad (3.12)$$

where $\tilde{E}_1 = \frac{D_1}{D_o}$ and $\tilde{E}_2 = \frac{D_2}{D_o}$ are the relative dilm density of the cloud at radii r_1 and r_2 respectively, and D_o is, as before the film density at $r = 0$. $\tilde{E}_1/\tilde{E}_2$ is D_1/D_2. (3.12) is equivalent to (3.10) when $\tilde{E}_1/\tilde{E}_2$ is equal to the equivalent surface density ratio, n_1/n_2. But we know from theory that D_1/D_2 is the ratio of functions of the logarithm of surface density, $\frac{f(\ln n_1)}{f(\ln n_2)}$, and mathematically these are not equivalent ratios. But, surprisingly, Manring's approximation can, under certain conditions, give equivalent magnitudes of the diffusion coefficient K. The condition under which (3.12) is equivalent to K values computed from (3.10) is shown in the following manner. (3.10) may be expressed

$$r_1^{\ 2} - r_2^{\ 2} = \sigma^2 \ \frac{(D_2 - D_1)}{\gamma} = \frac{4Kt \ (D_2 - D_1)}{\gamma}$$

Take $D_1 = \tilde{E}_1 D_o$ and $D_2 = \tilde{E}_2 D_o$, and solve for K, so that

$$K = \frac{(r_2^{\ 2} - r_1^{\ 2}) \ \gamma}{4t \ (\tilde{E}_2 - \tilde{E}_1) D_o} \qquad (3.13)$$

Equivalence of the two expressions (3.12) and (3.13), for K, requires

$$\frac{\gamma}{\hat{E}_1 D_o - \tilde{E}_2 D_o} = \frac{1}{\ln (\frac{\tilde{E}_1}{\tilde{E}_2})} \qquad (3.14)$$

or

$$\frac{\gamma}{D_o} = \frac{\tilde{E}_1 - \tilde{E}_2}{\ln\left(\frac{\tilde{E}_1}{\tilde{E}_2}\right)} \qquad (3.15)$$

The range in $\frac{\gamma}{D_o}$ that can be obtained for different combinations of $\tilde{E}_1$ and $\tilde{E}_2$ magnitudes is illustrated in Table 1.

		$\tilde{E}_2$			
		.2	.3	.4	.6
	.4	0.66	0.81		
$\tilde{E}_1$	.6	0.84	1.00	1.14	
	.8	1.00	1.18	1.33	1.62

Table 1. Magnitude of γ/D_o

The degree to which Manring's technique approximates the exact calculation of the diffusion coefficient, if γ is known, depends upon the choice of $\tilde{E}_1$ and $\tilde{E}_2$. For the types of films used in sodium trail photography (we may classify them as high gamma films ($\gamma \sim 0.4$) as in figure 1, a knowledge of the film type can be utilized to chose values of $\tilde{E}_1$ and $\tilde{E}_2$ so that Manring's technique would give consistently better approximations to the molecular diffusion coefficients computed from (3.10). This does not seem to have been noted previously. It may be mentioned in passing that Blamont and Baguette's, and Manring's approximation techniques are equivalent when $\tilde{E}_1 = 1$ and $\tilde{E}_2 = 1/e$.

In summary, none of the methods for obtaining the variance are without difficulties. This is especially so for the irregular trail below 108 km.

The method of central intensity is unsatisfactory because of the large column densities, n_0 associated with the trail axis. The maximum radius technique also has a greater applicability for small concentrations. For longer diffusion times (associated with larger concentrations) the background brightness changes are large; and the assumptions behind the technique no longer hold. The gradient log column density method assumes that the distribution of sodium vapor across a cloud diameter is a Gaussian function and its application is, at least, uncertain when the trail is of an irregular form. Some of these uncertainties are illustrated in the next section where we discuss the results of the relative dispersion computation for the different methods.

IV. DISCUSSION OF ANALYSIS

Figure 6 will serve to introduce our discussion of the nature of the sodium cloud expansion. This is a plot of molecular diffusion coefficients computed from sodium cloud photographs. They represent different seasons and different geographical locations. The dashed line in the figure represents the molecular diffusion coefficients computed by Rees (1961) from the theoretical formula (Chapman and Cowling, 1939)

$$K = \left\{ \frac{(3\pi^{\frac{1}{2}})}{16\rho} \cdot \left(\frac{2kT}{\mu}\right)^{\frac{1}{2}} \right\} \Big/ Q_d \qquad (4.1)$$

$$\mu = mM/m+M$$

The atmospheric number density, ρ, the mean molecular mass, M, and the temperature, T, are taken from the 1959 ARDC standard atmosphere. Q_d is the cross-section for diffusion.

The agreement between the theoretical curve and Manring's diffusion coefficient above 110 km is good, certainly within the 30% uncertainty that Rees (1961) suggests is associated with the magnitude of the diffusion cross-section Q_d. The diffusion coefficients reported by Rees and Blamont are greater than the theoretical, even allowing for the uncertainty in Q_d. We remarked earlier that, with low γ film (TRI-X), Blamont's technique should overestimate the magnitude of the diffusion coefficient by a factor of three or four. Correction for this would bring Blamont's values into closer agreement with the other studies. The two points ascribed to Rees (1961) are also greater than

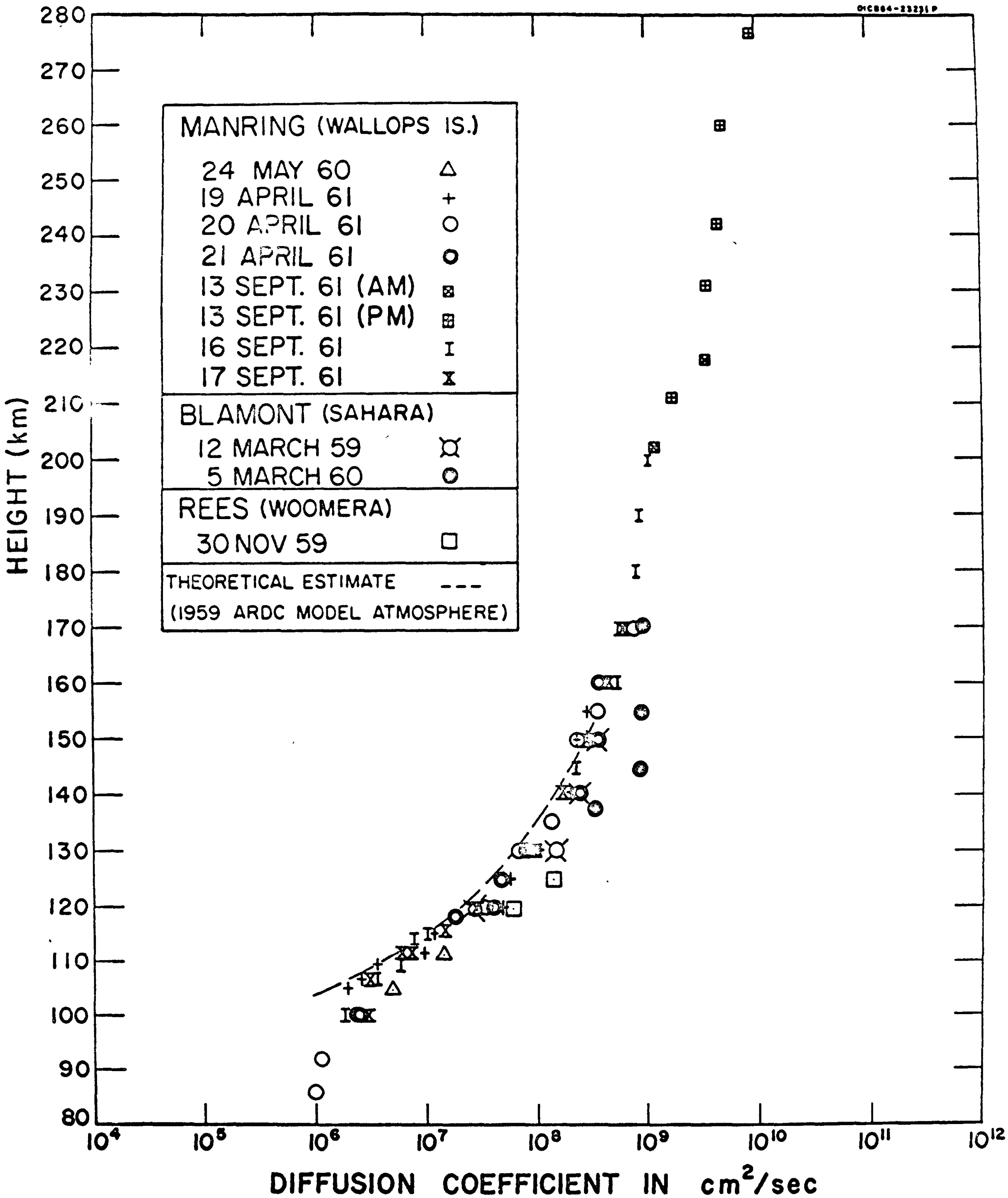

Fig. 6. The height variation in the experimental values of molecular diffusion coefficient.

the theoretical and serve to indicate the general magnitude of his measured coefficients.

Although he reported using a method similar to Blamont and Manring, no comment can be made about these points since he fails to indicate how he determined (or neglected) γ. Of interest to the question of turbulence is the indication that the measured diffusion coefficients in figure 6 begin to become much larger than the theoretical values below about 105 km.

One reasonthat there are so few determinations of diffusion coefficients below 105 is the irregular appearance of the trail. The gradient log "column" density method is of uncertain application when the distribution of film density across a diameter has two or three peaks and is highly non-Gaussian. Even in instances when the irregular appearance ceases at heights of 100 to 102 km there can still be an uncertainty in the calculation of σ^2 from cloud photographs greater than 7 to 8 minutes after cloud formation. This point is illustrated in figure 7. In that figure we plot three measurements for each densitometer trace: the measured r_e^2 values ($\odot$), the measured r^2 at .368 D_o (+) (Blamont's technique for approximating σ^2), and $\frac{\sigma^2}{\gamma}$ values computed by the gradient log "column density" method (Δ). The measurements represented by these points are made at a height of 107 to 108 km where the cloud image has a smooth appearance. It is evident from figure 7 that r^2 at D_o/e follows closely the variations of the visible radius squared as is expected.

In figure 7 an apparent discontinuity in the three different sets of measurements between 280 seconds and 310 seconds is also evident. The "discontinuity" between the Δ points is not considered to be significant in view of the obvious scatter of the Δ points in figure 7 (see discussion to follow

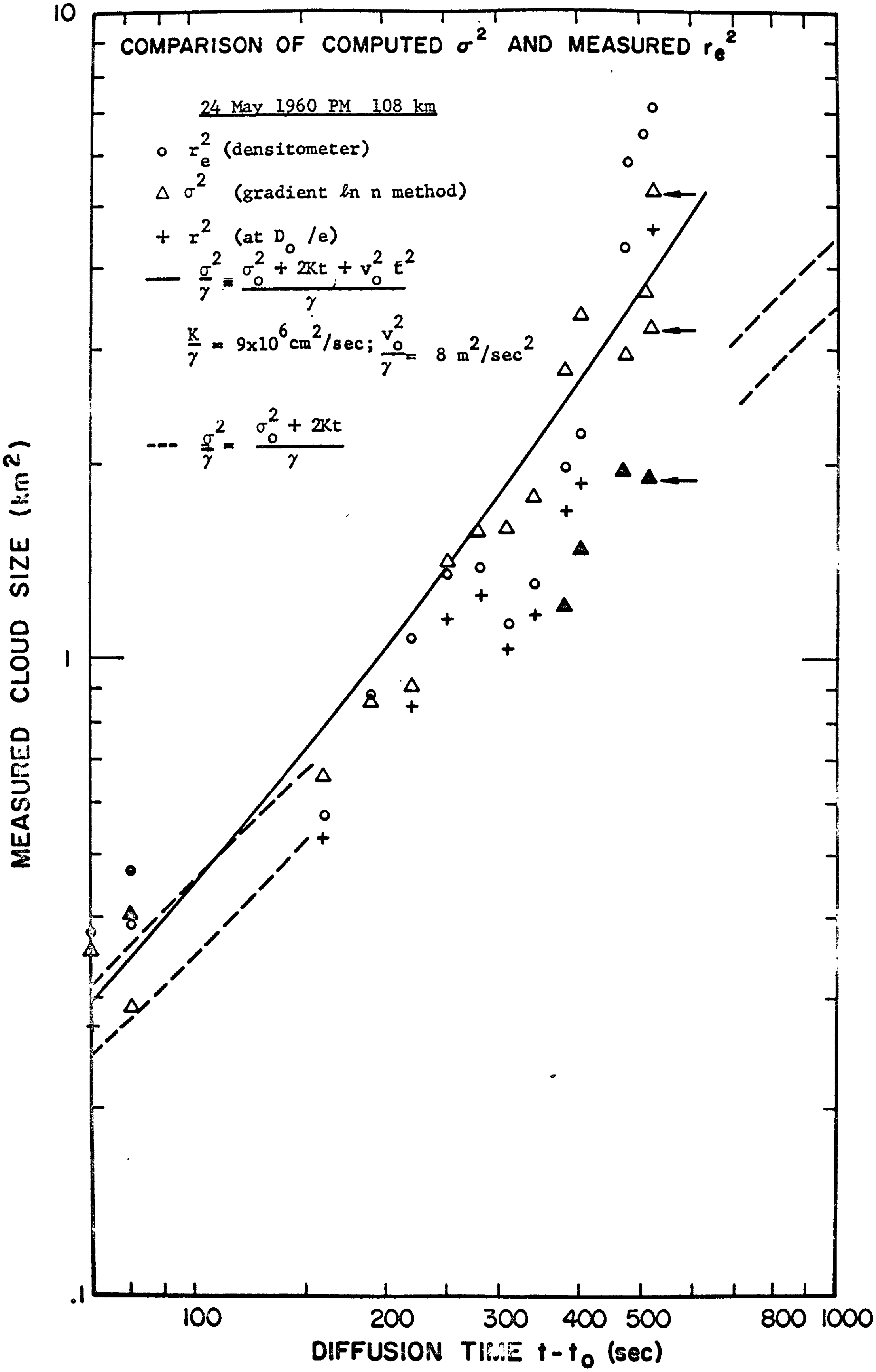

Fig. 7. A comparison of the measured visible radius squared with computed values of the cloud variance, σ^2, for the evening twilight of 24 May 1960. The equivalent height of the cloud is 108 ± 1 km.

on the large scatter between the "dark" and "light" delta values for 380 to 515 seconds). Both sets of r^2 points (o and +) at 310 and 340 seconds are about 25% lower than the general trend of other sets just prior to and after them in figure 7. By a similar percentage they are also lower than the other more numerous r_e^2 points (of the same section of cloud and from the same negatives) illustrated in figures 9 and 10. An explanation of this "discontinuity" would run as follows. For the r_e^2 and r^2 (at D_o/e) values in figure 7, we consistently select the minimum visible diameter from the densitometer trace whenever we are uncertain about the film density level representing the sky background and cloud intersection. Furthermore, the magnitude of the minimum r_e^2 points plotted in figure 7 at 310 seconds is about 25% less than a maximum possible magnitude, $r_e^2 = 1.56$ km^2. The 25% figure is one estimate of the possible uncertainty in r_e^2 (for a given time) when there is an uncertain definition of the "visible" cloud diameter. Why is this more evident in the r^2 points (o and +) at 310 and 340 seconds? The most plausible answer to this question involves camera stop changes. Unfortunately the camera operator's log for these particular photographs does not indicate when stop changes were made and our answer, although plausible, is nevertheless hypothetical. (see Note 1, page 63)

The computation of $\frac{\sigma^2}{\gamma}$ was terminated at 515 seconds because of the wide range in $\frac{\sigma^2}{\gamma}$. The extent of this range is illustrated in figure 7 by the two delta values at each of 380, 400 and 470 sec and the three delta values at 515 sec. The three arrows aid in identifying these latter three delta points. The lowest solid delta point in each instance is the lowest magnitude of $\frac{\sigma^2}{\gamma}$ for the particular densitometer trace. This variation in $\frac{\sigma^2}{\gamma}$ (for a given time) results from the dependece of the difference ratio $\frac{\Delta D}{\Delta r^2}$ on D (which is characteristic of a non-Gaussian D vs

r^2 curve). For a Gaussian shaped D-curve, the differential, $\frac{\Delta D}{\Delta r^2}$, used to evaluate $\frac{\sigma^2}{\gamma}$, is independent of D.

From this brief comparison of r_e^2, $.368\ r_e^2$, and $\frac{\sigma^2}{\gamma}$ in figure 7, it is evident that the time period of most interest to the problem of turbulent expansion of sodium cloud corresponds with the time period of cloud expansion about which there is the most uncertainty concerning the magnitude of $\frac{\sigma^2}{\gamma}$. The r_e^2 points in figure 7 (and in later figures also) indicate a more rapid growth than can be explained by molecular diffusion alone. The $\frac{\sigma^2}{\gamma}$ points between 380 and 515 seconds could be interpreted in either of two ways depending upon whether the maximum (Δ) or minimum ($\blacktriangle$) values of $\frac{\sigma^2}{\gamma}$ are valid. With the minimum values the general growth of $\frac{\sigma^2}{\gamma}$ is linear in time. This is indicated by dashed lines running out from the boundaries. The range of diffusion coefficient represented by these dashed lines is $8.8\ \gamma \times 10^6\ cm^2/sec$ (lower) and $\gamma \times 10^7\ cm^2/sec$ (upper). The maximum values of $\frac{\sigma^2}{\gamma}$ are well fitted by the solid curve in figure 7 which represents

$$\frac{\sigma^2}{\gamma} = \frac{\sigma_o^2 + 2Kt + V_o^2\ t^2}{\gamma}$$

where $\frac{K}{\gamma}$ is $9 \times 10^6\ cm^2/sec$ and $\frac{V_o^2}{\gamma}$ is $8\ m^2/sec^2$.

Even if the upper Δ are valid, changes in γ could make possible a $\sigma^2 \sim t$ relation. When γ is constant, it should be about 0.8 in this case. Otherwise it is a decreasing function of time (through changes in ln E with time). Without more precise quantitative information on, first, the absolute magnitude of the sky background, secondly, onthe aperture setting of the camera, and finally on the combined effect of both of these on γ, we must recognize the possibility that γ may have a t^{-1} dependence so that $\frac{\sigma^2}{\gamma} \sim t^2$ may still be $\sigma^2 \sim t$.

In a subsequent analysis of the average r_e^2 values for this cloud (in this section) we shall obtain a t^3 dependence for the relative dispersion where we know qualitatively that both the changing sky background brightness and distortion of the cloud by wind shear enhance the apparent cloud expansion rate. Since these effects do not influence, to the same degree, the determination of $\frac{\sigma^2}{\gamma}$ by the gradient ln (n) method, it is of importance to our understanding of the time dependent nature of sodium cloud dispersion that further effort be made to obtain reliable estimates of $\frac{\sigma^2}{\gamma}$ from the non-Gaussian D vs r^2 curves for late diffusion time.

Although we cannot, at this time, obtain, by the gradient ln n method, information on trail dispersion for times greater than 500 seconds, we can use (3.1) to draw inferences from the r_e^2 data beyond 500 seconds. We shall assume the form of the relative dispersion, either turbulent, molecular, or both, and solve for parameters by fitting theoretical r_e^2 curves to measured r_e^2 point. It is recognized that we are forfeiting, in this instance, our ability to use the data to generate their own dispersion statistics. But, in view of comparisons with other studies to be made in section V, there is a need for comparable values of turbulence parameters. Furthermore this is a useful technique for emphasizing the difference between dispersive and non-dispersive changes in a cloud image.

In a Gaussian cloud, it follows from (3.1) that the visible radius squared may be represented by the following formula

$$r_e^2 = 2\sigma^2 \left[\ln \frac{N}{\mu n_e} - \tfrac{1}{2} \ln(2\pi\sigma^2) \right] \qquad (4.2)$$

We assume that the relative dispersion, σ^2, is mean square additive; the turbulent dispersion is represented by either of the two theoretical predictions of the form of its dependency: $\sim t^2$ or $\sim t^3$; and molecular dispersion is represented for a cylindrical cloud by 2 Kt. As summarized in section 2.B the two forms of σ^2 which result from these assumptions are

$$\sigma^2 = \sigma_o^{\ 2} + 2Kt + v_o^{\ 2}\, t^2 \qquad (4.3a)$$

$$\sigma^2 = \sigma^2 + 2Kt + 2/3\, \tilde{B}\, t^3 \qquad (4.3b)$$

If we make plausible assumptions about the numerical magnitudes of the variables $\frac{n_e}{N}$, K, and $\tilde{B}$ or $v_o^{\ 2}$, compute theoretical curves of $r_e^{\ 2}$ vs time, and compare the fit of the computed curve with the measured values, it is possible to draw some limited inferences about our original assumptions concerning $\frac{n_e}{N}$, K, and $\tilde{B}$ or $v_o^{\ 2}$.

Physically, we parameterize all of the optical effects into the factor $\frac{n_e}{N}$: changes in background intensity, changes in γ, changes in atmospheric attenuation at 5893 Å, and changes in μ. All dispersive effects on $r_e^{\ 2}$ are included in the σ^2 variable. But since we do not let $\frac{n_e}{N}$ change with time, the only way that we can determine whether or not background and other non-dispersive changes are influencing the visible size of the cloud, is by displacement of the measured points from the computed curves. With increasing time, the measured $r_e^{\ 2}$ values should cross from one constant value $\frac{n_e}{N}$ curve to another. For late diffusion time in an evening twilight the measured points should cross from high to low values of $\frac{n_e}{N}$ to reflect the decreasing background brightness; for late diffusion time in a morning twilight the measured points should cross from low to high values of $\frac{n_e}{N}$.

In order to determine a plausible magnitude for $\frac{n_e}{N}$, we consider the natural atomic abundance or column density. Chamberlain (1961) summarizes a number of twilight observations, and indicates that the natural background column density of sodium against which the clouds are photographed varies from 10^9 to 10^{10} atoms/cm^2. We choose the upper value of 10^{10} to be the surface density defining the edge of a visible (photograph) cloud. For linear trail density, N, we take 10^{17} atom/cm (see page 24). This gives us an approximate value of 10^{-7} cm^{-1} for $\frac{n_e}{N}$.

The late diffusion time r_e^2 measurements for 24 May 1960 [the same cloud analyzed in figure 7] are shown in figure 8. The curves in figure 8 represent the theoretical growth of r_e^2 computed from (4.2) with assumed values for $\frac{N}{n_e}$ and with σ^2 represented by (4.3b). The differences between the five curves in figure 8 result from different assumed magnitudes for $\frac{n_e}{N}$ and $\tilde{B}$, since all curves are computed with μ of unity, an assumed K of 10^6 cm^2/sec, and a σ_o^2 of 22 x 10^4 cm^2. The great majority of points are bounded by curves (4) and (3) representing a range of $\frac{n_e}{N}$ from 4 x 10^{-7} to 4 x 10^{-8} cm^{-1} and a value of 90 erg/g sec for $\tilde{B}$. The general trend of measured r_e^2 is from curve (4) (for microscope measurements ⊙) and from curve (2) (for densitometer measurements (+)) to curve (3) very soon after 500 seconds. The observed drift of the measured r_e^2 values toward r_e^2 curves computed with smaller values of $\frac{n_e}{N}$ represents the combined effect of decreasing sky background and atmospheric dispersion. If there were no changes in sky background the turbulent contribution to σ^2 would be represented by a t^4 or t^5 dispersion law. (With a t^5 or t^4 law in (4.2) the resulting r_e^2 curve would grow at a steeper rate and therefore give a better fit to the measured r_e^2 values.) Furthermore, the

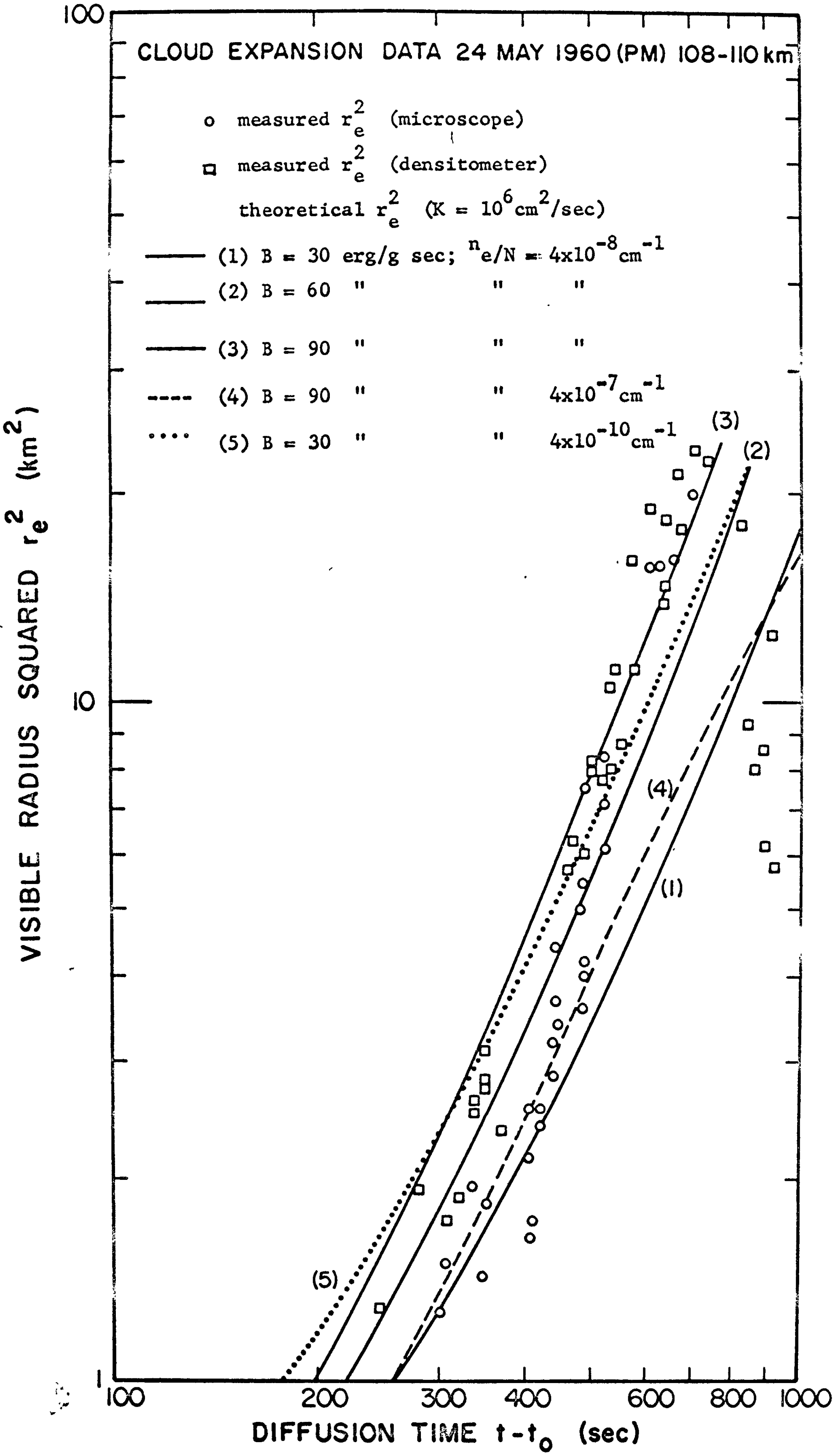

Fig. 8. Variation in time of the measured visible cloud radius squared and theoretical curves of the visible radius squared (4.2). The equivalent height is 108 ± 1 km for the evening twilight cloud of 24 May 1960.

value of $\bar{\mu}$, which we have taken to be unity, is also a time dependent function which interacts with the changing sky background through the product $\frac{N}{\mu n_e}$ in (4.2). For the 24 May measurements μ is a linear function of time, but one whose magnitude decreases and then increases in a complicated manner. The variations in μ are accessible from the photographic data and, with some additional effort, they can be evaluated when the wind field is obtained from the cloud photographs.

For comparison with the 24 May evening twilight cloud (4.2) is applied to the 17 September 1961 morning twilight cloud. In figure 9 the two solid curves represent theoretical r_e^2 values in which the turbulent form of the dispersion is assumed to be $v_o^2 t^2$. These computed r_e^2 curves have values of v_o^2 equal to 4 m^2/sec^2 and 2 m^2/sec^2 and values of $\frac{n_e}{N}$ equal to 4×10^{-7} cm^{-1} and 4×10^{-8} cm^{-1} respectively. These $\frac{n_e}{N}$ magnitudes are chosen because they represent the most probable extreme values (see page 24).

In figure 9 the measured r_e^2 values for 24 May 1960 (densitometer only), 17 September 1961 (densitometer and microscope), and 20 April 1961 (microscope) are also plotted. (The theoretical r_e^2 curves computed with the $\frac{2}{3}\tilde{B}t^3$ assumptions are illustrated in figure 8 and may be reviewed by references to that figure.) The densitometer traces, represented by the r_e^2 points for 17 September and 24 May, were taken with care and particular emphasis on determining the visible radius, r_e.

The r_e^2 values for 20 April 1961 represent an average of ten different visual measurements between "a" and "b" in figure 4 (Wallops Island negatives). Although the total length of the photographic sequence is too short to allow a distinction between either the t^2 or t^3 dispersion law, the r_e^2 do establish

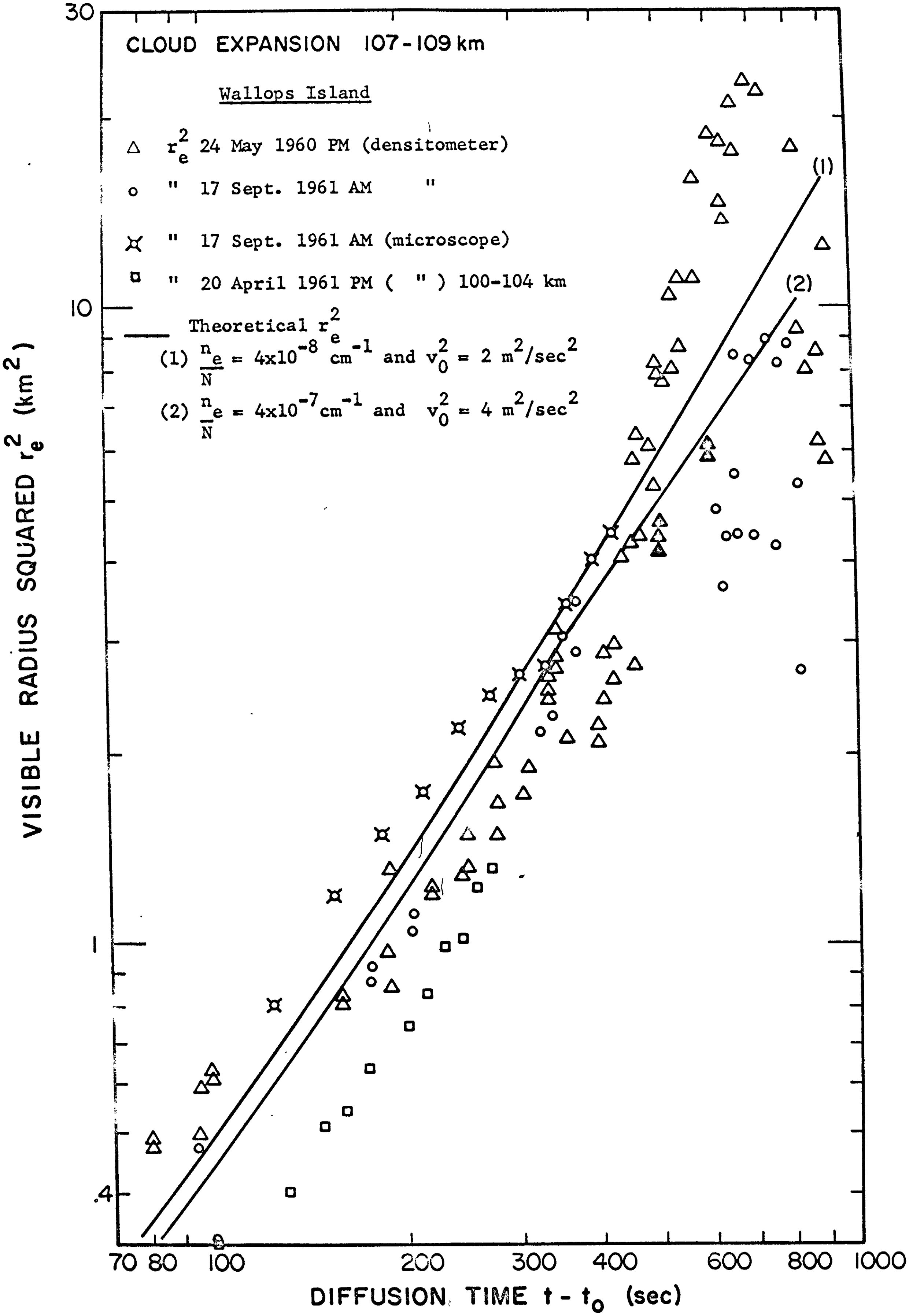

Fig. 9. Variation in time of the measured visible cloud radius squared and theoretical curves of the visible radius squared. The measured visible radii squared are for the twilight clouds of 24 May 1961, 20 April 1961, and 17 September 1961. The equivalent cloud heights are between 100 and 109 km.

a constraint on σ^2. Whatever the assumed functional form of σ^2 in (4.2), it must result in an approximate t^2 growth for $r_e^{\,2}$ between 100 and about 300 seconds.

Beyond 400 seconds the divergence in the $r_e^{\,2}$ growth for the 17 September morning twilight cloud and the 24 May evening twilight cloud is very evident in figure 9. Ignoring the effect of changing sky background brightness on the magnitudes of $r_e^{\,2}$, these two sets of measurements suggest for one cloud an effective relative dispersion ~ t^2 and one certainly greater than t^3 for the other (see figure 8). Bringing background brightness changes back into consideration we can only suggest, since we have no quantitative estimates, that the relative dispersion after 400 seconds is something less than t^4 and greater than or equal to t^2. It is also worth noting, for those tempted to cite the existence of atmospheric turbulence on the basis of cloud morphology (Edwards et. al., 1963; Blamont and de Jager, 1961; Rees, 1961), that a smooth "non-turbulent" cloud appearance can also be associated with accelerated cloud growth.

Of further interest in figure 9 is the spread between the microscope (Wallops Island) and densitometer (Andrews Air Force Base) measurements for the 17 September cloud. These measurements represent the size of the same cloud mass (107 to 108 km) but for a different viewing angle and different combination of camera lens and film. Unfortunately we have no way to apportion the cause of this systematic difference in $r_e^{\,2}$ between differences in camera site location: range, viewing angle, etc., and differences in measurement technique: microscope and densitometry.

The rate of growth of the two P.M. clouds (different heights) of 20 April and 24 May could be fitted more closely to theoretical r_e^2 curves if, with the same values of $\frac{n_e}{N}$, r_e^2 is computed using v_o^2 equal to 1 and 2 m^2/sec^2. This suggests that 2 to 4 m^2/sec^2 can be considered representative of an effective mean square velocity associated with the sodium cloud growth. Even the 24 May r_e^2 points would support this estimate if the following quantitative demonstration could be made. The solid triangles in figure 9 represent r^2 at a film density level .1 above the sky brightness film density level. If this magnitude film density change corresponds with the actual changes in sky background, then the t^2 dispersion law would be confirmed. This demonstration involves quantitative knowledge of both sky brightness and film sensitivity changes.

In the concluding analysis we consider the maximum radius technique. For the morning twilight sequence of September 17, 1961, σ^2 values are computed from an arbitrary selection of measured r_e^2 values (at the 108 $\pm$ 1 km height). The σ^2 values are computed from equation 3.8. (3.8 is similar to equation 4.2 which is used to compute the r_e^2 curves in figure 9. The difference is that $\frac{n_e}{N}$ in 4.2 is replaced in 3.8 by the $\frac{n_e}{N}$ value determined by 3.7). Figure 10 illustrates the results of this computation in which the maximum radius squared, ρ^2, is 14 km^2 (ρ^2 is represented by the Δ point at 810 seconds). The four σ^2 values between 200 and 700 seconds may be fitted to a $\sigma^2 = v_o^2 t^2$ curve (dashed) for which $v_o^2 \sim$ [illegible]m^2/sec^2. The two early points at 55 and 85 seconds are slightly above the dashed curve which is to be expected from the increasing relative importance of molecular dispersion in the total dispersion, σ^2, as $t \to o$.

The last Δ point, representing ρ_4^2 is displaced well above the intersection of the solid curve, representing $\sigma^2 = v_o^2\ t^2$, and the 810 second abscissa line. This displacement could indicate a transition to turbulent dispersion with a higher power time dependence, if the sky background were constant, or a premature contraction of the visible cloud due to increasing sky brightness. The late time deviations of the measured r_e^2 points (o) from curve (1) in figure 9 are an example of the latter. This is better illustrated by the accompanying inserted drawing. The full lines represent an actual measured r_e^2 curve and a computed σ^2 curve. One dashed line represents the measured r_e^2 points if there had been no increase in sky brightness; the other dashed curve represents the corresponding σ^2 values computed from 3.8. The increasing sky brightness causes the maximum radius to be measured at time t_2 rather than t_3.

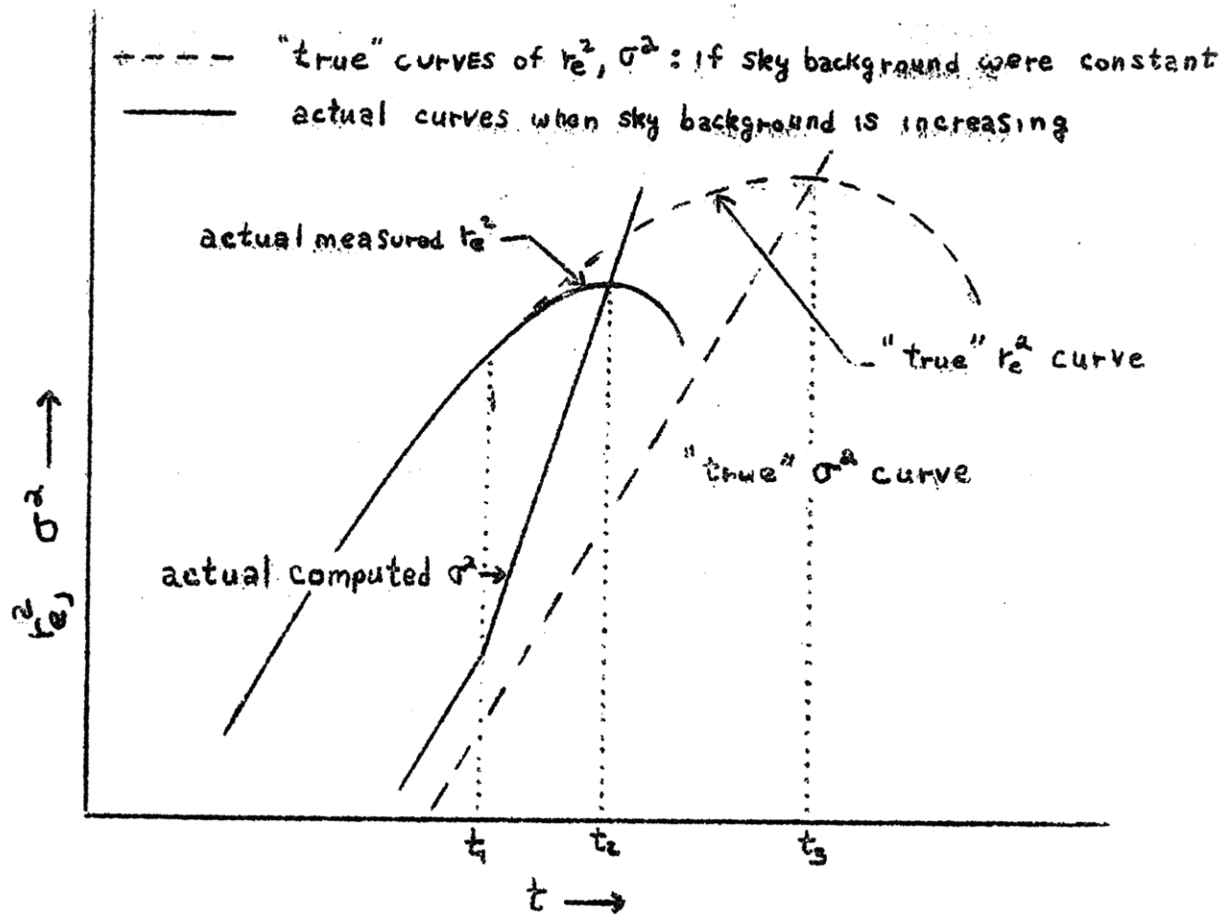

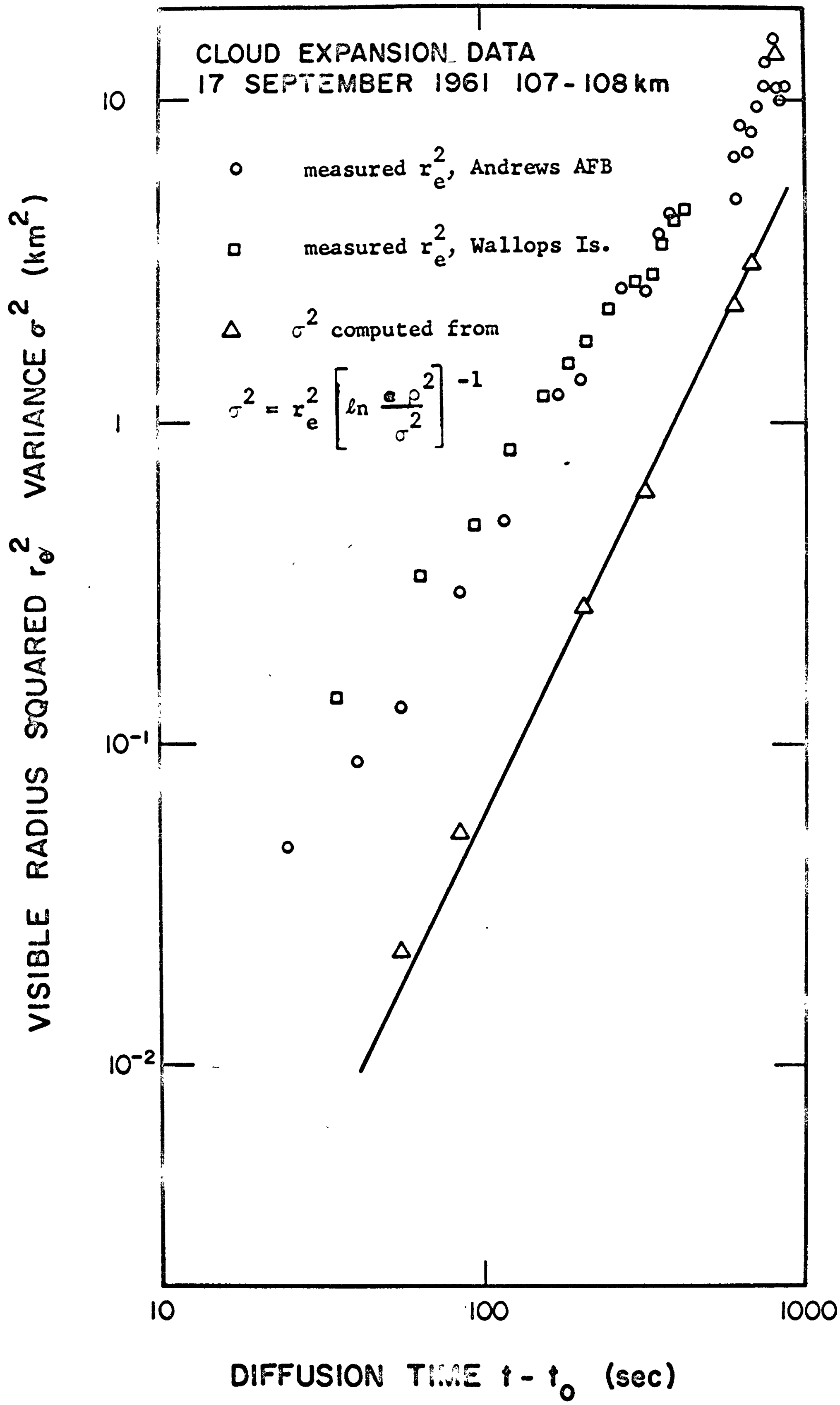

Fig. 10. Variation in time of the measured visible radius squared and the variance , σ^2, computed from the maximum cloud radius. The equivalent height is 108 km for the morning twilight of 17 September 1960.

and the effect on computed σ^2 is seen to be a displacement of these values above the "true" dashed curve after time t_1. (Note: "true" values are those values which would have been observed or computed had the sky background brightness actually been constant with time.)

This reduction in the magnitude of the "true" σ^2 values below the actual computed σ^2 values can be illustrated with the sodium data. In figure 11 the circles represent averaged measured r_e^2 (microscope) from Wallops Island negatives for 9 December (figure 6a). The height of the cloud is 116 to 117 km and is considered sufficiently high so that molecular diffusion dominates the cloud growth. Two different values, 3.48 and 4.68 km^2, are assumed for the maximum visible radius and they are represented by ⊙ and ☒ respectively in figure 11. (No uniqueness is attached to these values.) For the sake of this hypothetical example, 3.48 km^2 is the observed maximum radius and 4.68 km^2 is the "true" maximum radius. From equation (3.8), values of σ^2 are computed from each of the (○) points for both assumed values of the maximum r_e^2. The individual σ^2 computed with 4.86 km^2 (Δ) are less than those computed with 3.48 km^2 (□). The Δ points at earlier times ($t < 200$) are seen to fit a molecular diffusion law (the straight lines represent $\sigma^2 \sim t$). At later times there is a greater growth of the (□) points than the linear law. This is quite pronounced for the points computed with the smaller of the two assumed radii. The (□) points suggest a higher power time dependence than molecular diffusion which is a spurious result.

This demonstration of the increasing sky background effect illustrates how important it is, in diffusion studies, to consider optical effects.

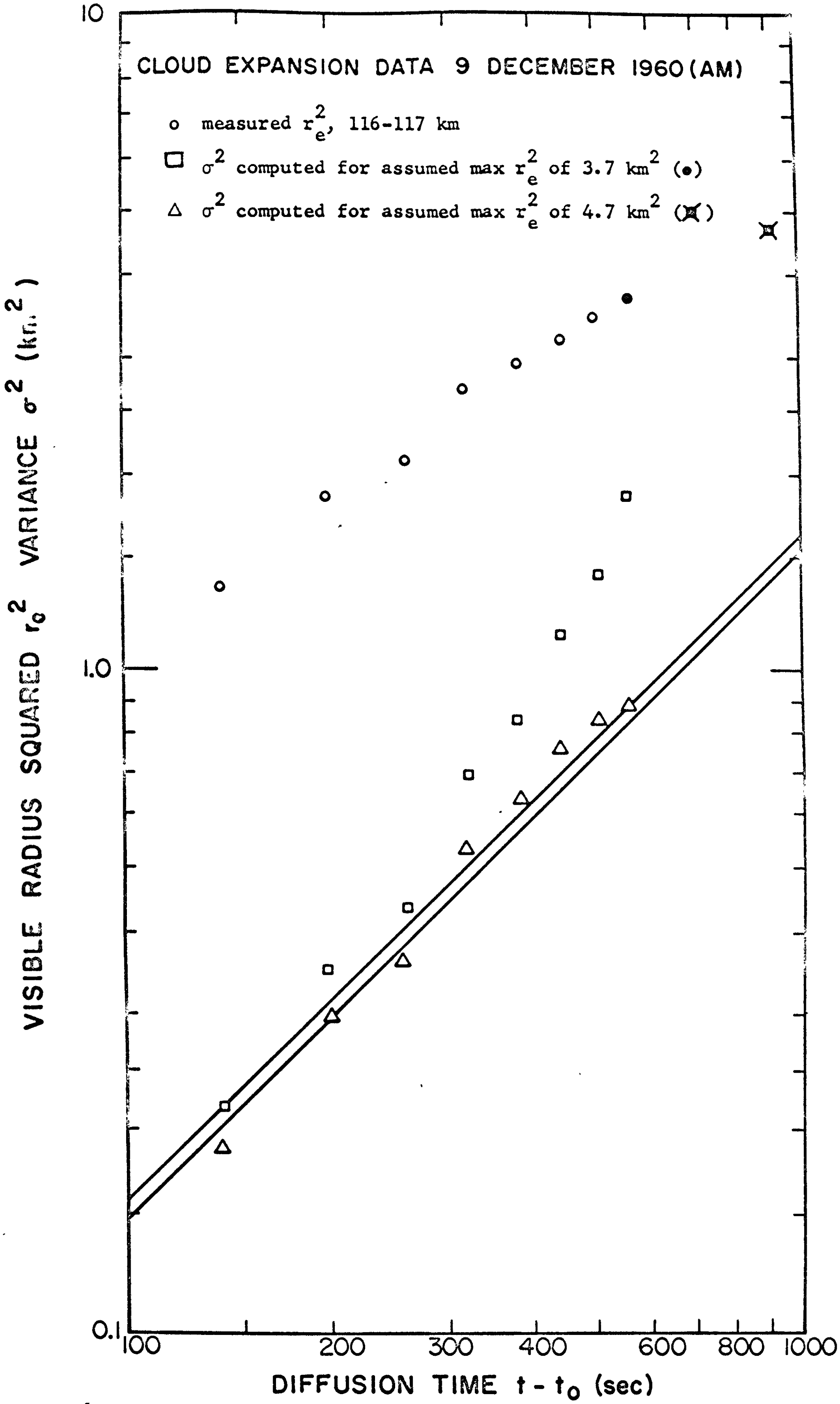

Fig. 11. Variation in time of the measured visible radius squared and variance computed from two assumed values of the maximum cloud radius squared, r_e^2 = 3.7 and 4.7 km . The measured r_e^2 are at 116 to 117 km for the morning twilight cloud of 9 December 1960.

How do we summarize the previous anlaysis? The application of the maximum radius method (figure 10) to the 17 September A.M. cloud results in a relative dispersion, $\sigma^2 \sim t^2$, for t up to 620 seconds. Beyond that time the departure of the computed σ^2 from the $\sigma^2 \sim t^2$ relation is consistent with changes in sky brightness, and does not necessarily indicate a transition to a higher order dispersion law. The result of the gradient ln n method is less definite. Either a t or t^2 dependence for σ^2/γ is indicated. Finally the application of (4.2), as evidenced in figures 8 and 9, indicates a t^3(possibly t^4) dependence when the cloud expands against a decreasing brightness and t^2 dependence when it expands against an increasing background brightness. In both instances the films are high γ (therefore smaller range of ln E over which γ is constant). Quite definitely, we should expect an influence of non-constant γ in these results.

Taken altogether, these results indicate that the most probable form of the accelerated diffusion is $\sigma^2 \sim t^2$ with a slight possibility that either a t^3 or t could result when the effects of the changing background brightness and film sensitivity are considered quantitatively.

V. COMPARISON WITH PREVIOUS STUDIES

Other studies of alkali vapor cloud expansion have been published by Blamont and De Jager (1961), Noel (1963), and Zimmerman and Champion (1963). Blamont and De Jager have determined cloud expansion from photographs of a sodium vapor trail. In the other two studies the expansion of cesium vapor clouds has been determined from photographs obtained during Project Firefly experiments (Rosenburg, 1959; 1960).

Blamont and De Jager measure the expansion of a morning twilight sodium cloud from 60 to 120 seconds after cloud formation. The height at which this expansion occurs is not stated but may be inferred, from other remarks in their study, to be below 102 km. During the sixty seconds between measurements the average cloud "diameter" increased from 90 to 500 meters. To these two "diameters" and a sequence of four meteor trail "radii" measured by Greenhow (1959), Blamont and De Jager fit the relation $\sigma^2 = 4/3 \in t^3$. The approximate magnitude of $\in$ is 70 erg/g-sec, the same value obtained by Greenhow (1959) from meteor trail expansion at 90 km.

By this procedure, Blamont and De Jager implicitly assume that the standard deviation, σ, is to a good approximation, equal to their average visible cloud "diameter". This is usually not a good assumption, as shown in connection with the determination of molecular diffusion coefficients (see page 28). That Blamont and De Jager obtained an estimate as low as 70 erg/g sec is surprising when we consider the much larger estimates that would be obtained by using their method with Wallops Island sodium trail data for comparable altitudes.

For example, if this technique of Blamont and De Jager is used to obtain an estimate of ϵ in figure 8, the same relation, $\langle r^2 \rangle = \frac{4}{3} \epsilon t^3$, would require an ϵ of about 430 erg/g-sec to fit the measured r_e^2 points. This contrasts with the 15 to 45 erg/g-sec range of ϵ associated with the theoretical r_e^2 curves in figure 8, when $\frac{4}{3} \epsilon t^3$ is substituted for $\frac{2}{3} \tilde{B} t^3$. Thus, there is a difference of about a factor of ten between the ϵ value obtained from the r_e^2 data in figure 8, using the Blamont and De Jager approximation, $\sigma^2 \sim r_e^2$, and using (4.2) with $\frac{4}{3} \epsilon t^3$ as the turbulent form of the relative dispersion.

There is, of course, an inverse relation between assumptions about the form of σ^2 and the magnitude $\frac{n_e}{N}$ in (4.2). Certainly the more accurate our knowledge of the $\frac{n_e}{N}$, the better will be our determination of the form of σ^2. With sodium clouds, the value of n_e defining the minimum cloud intensity, just distinguishable against the natural sky background, is taken to be the natural sodium abundance which is well known from a large number of twilight airglow studies (Chamberlain 1961; Donahue and Foderaro, 1954). This knowledge gives us some confidence in the use of (4.2) with sodium cloud expansion data. With cesium clouds, discussed in the next paragraph, the number of cesium atoms per square centimeter column, whose brightness is equivalent to the natural sky background at 8521Å, would have to be estimated.

In the other studies of alkali metal clouds, both Noel (1963) and Zimmerman and Champion (1963) study the expansion of cesium vapor clouds. These are extremely energetic releases (see Groves, 1963), in which visible cloud diameters are of the order of 1 km within tenths of seconds after the explosive burst which vaporizes the cesium (Rosenberg, 1959). All these clouds are initially spherical but through wind shear they assume, over a three to four kilometer depth of atmosphere, the appearance of a trail within approximately two minutes after the time of burst.

Noel, in his study, measures the visible radii of small "globular" masses within the cloud. These vary in height from 104 to 109 km. To the values of the measured visual radii squared Noel also fits a $\frac{4}{3} \in t^3$ curve, and obtains an average value of $\in$ equal to 320 erg/g sec. Noel's four sets of measured r_e^2 values and, for comparison, measured r_e^2 values for the 17 September 1961 Wallop Island trail are plotted in figure 12. In addition, we have averaged the respective r_e^2 for the three sets of Noel's points that all have values at 255, 315 and 375 seconds. These average points are represented by the Δ's in figure 12. The solid curves in figure 12 are computed from (4.2) with $\sigma^2 = \sigma_o^2 + 2Kt + \frac{4}{3} \in t^3$ to agree with Noel's assumption. If the $\frac{n_e}{N}$ are comparable for both cesium and sodium clouds (and there is some evidence for this, (Manring, 1961), then and fit of the Δ points to curve (1) in figure 12 indicates that Noel's assumption of $r_e^2 \sim \sigma^2$ can overestimate the turbulence parameter $\in$ by a factor of ten ($\in$ in curve (1) is 30 erg/g sec). Furthermore Noel's t^3 growth curve for cesium "globs" contrasts with our estimate of a t^2 growth for the 17 September sodium trail (the $-|-$ points in figure 12).

Since they do not represent the actual visible cloud radius squared but, instead, the visible radius squared of smaller "globs" of cesium vapor within the cloud itself (Noel, 1964), there remains some question concerning the isophote level associated with the successive measurements of "glob" size. With the actual visible cloud diameter the sky background brightness determines the isophote level. Although it is changing, it can be determined. The question

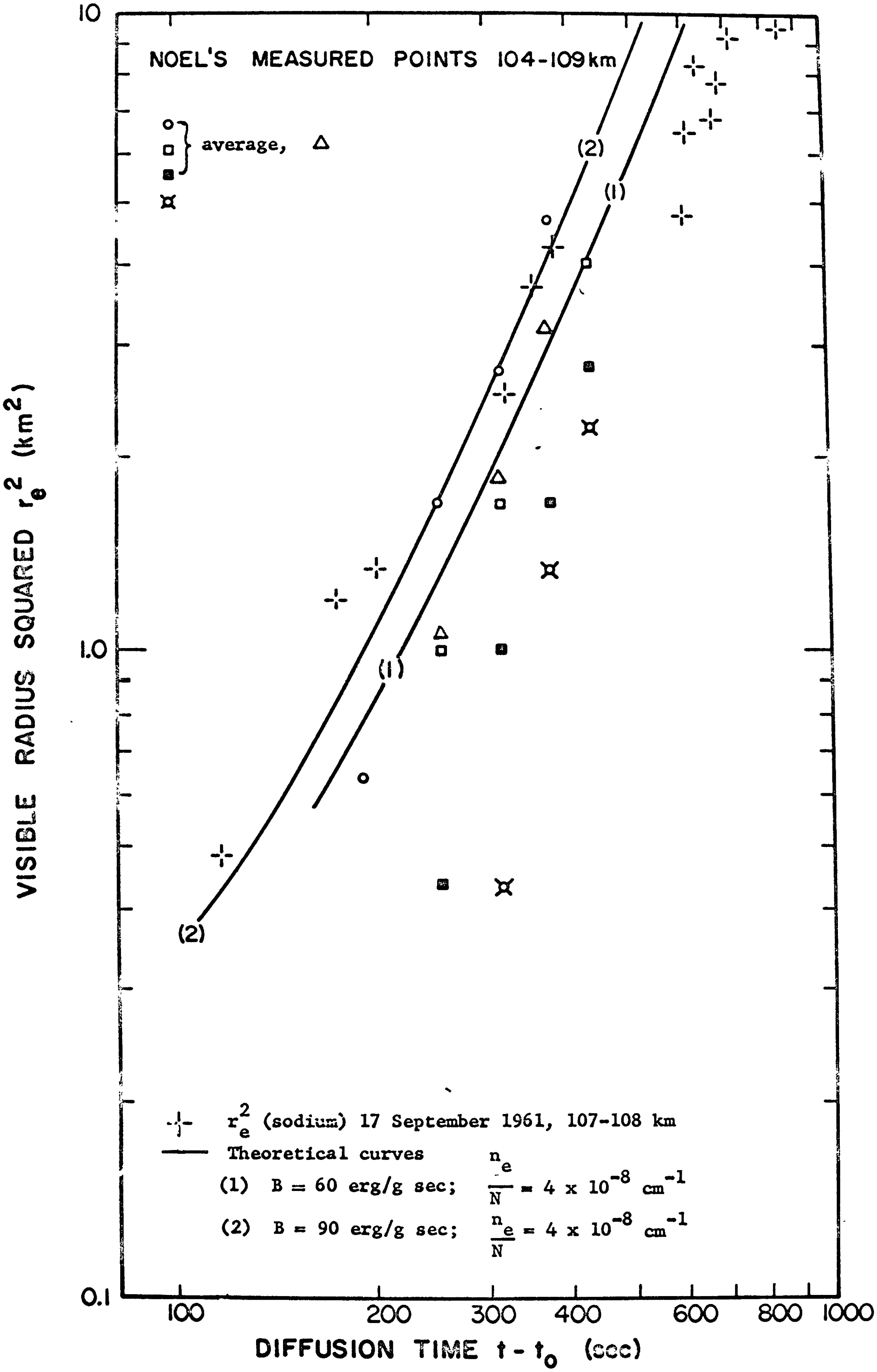

Fig. 12. Variation in time of measured visible radius squared and theoretical curves of visible radius squared. A comparison of Noel's (1963) measurements of cesium clouds with the morning twilight cloud of 17 September 1961. The equivalent heights are 104 to 107 km.

is raised because Noel's measurements very definitely indicate a $\sigma^2 \sim t^3$ relation for a morning twilight cloud, in contrast with other cesium cloud analyses by Zimmerman and Champion (which follow) and with our analysis of the 17 September A.M. sodium cloud expansion.

Zimmerman and Champion measure the cloud growth for three cesium vapor clouds from the 1959-1960 Project Firefly Series. The measured r_e^2 values for two of these morning twilight clouds, "Echo" and "Bravo", are plotted in figure 13. The straight solid lines in figure 13 represent curves for which the radius squared is proportional to the first power of time. There is an interesting contrast in cloud growth between the measurements for "Echo" and "Bravo". The height of cloud "Echo" is 100 $\pm$ 1 km; the height of cloud "Bravo" is 112 $\pm$ 1 km. (Rosenberg 1959).

"Bravo" expands up to about 300 seconds at an apparent rate that is slightly less than the straight t curve. Beyond 300 seconds the growth accelerates markedly. Although Zimmerman and Champion do not comment upon this behavior, it should be studied further to verify that it is a real effect of the dispersion of the cesium vapor by atmospheric motions. These measurements were made above 110 km. Above that height the behavior of sodium clouds suggests that molecular dispersion predominates. The validity of these measurements have a real importance to our understanding of atmospheric dispersion at these heights.

For the lower cloud, "Echo" (height about 100 km) the growth may, on the one hand, be interpreted as fitting the lower $r^2 \sim t$ curve drawn in figure 13 up to 100 seconds, and the middle $r^2 \sim t$ curve after 200 seconds. The accelerated growth rate occurs between 100 and 200 seconds, and it, again may reflect

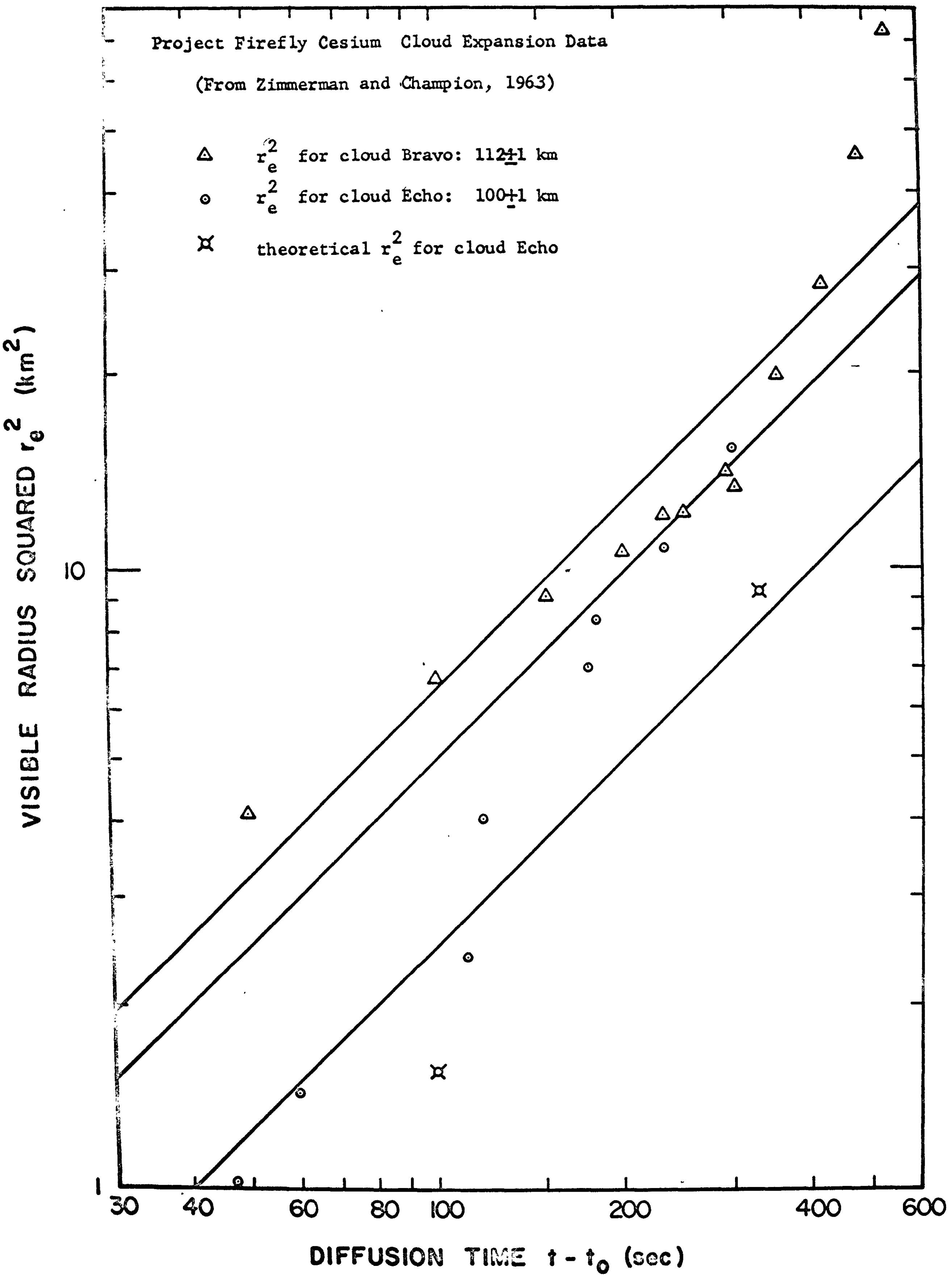

Fig. 13. The measured visible radius squared for two cesium vapor clouds. The equivalent heights are 99 ± 1 ("Echo") and 112 ± 1 ("Bravo"). (After Zimmerman and Champion, 1963)

either a dispersive or an optical effect (such as changes in exposure time or stop number).

On the other hand, the "Echo" r_e^2 values may be interpreted in terms of a $\sigma^2 \sim t^2$ growth law, not just between 100 to 200 seconds. Zimmerman and Champion assume that Tchen's prediction for relative dispersion (large mean shear flow case) is valid and take σ^2 equal to $v_o^2\ t^2$. They assume a maximum r_e^2 of 20.25 km^2 (no r_e^2 values of this magnitude are actually reported by them). Instead of computing σ^2 for each r_e^2 as we do in figure 10, they essentially use the maximum radius to evaluate $\frac{n_e}{N}$ in equation 4.2, assume v_o^2 is equal to 15 m^2/sec^2, and compute r_e^2 at 100 and 330 seconds. Their theoretical r_e^2 values are indicated by the ☒ symbol in figure 13. They report that "the calculated values [of r_e^2] agree with [measured r_e^2] values."

Zimmerman and Champion's analysis of the "Echo" measurements could have been performed with more care. They do not show that the maximum r_e^2 is actually measured. Otherwise, if it has not been measured, any other value a little higher or lower is of equal validity to 20.25 km^2, which, in turn, would result in a higher or lower evaluation of $\frac{n_e}{N}$. Assuming that 20.25 km^2 is actually measured by them, the agreement between computed r_e^2 and measured r_e^2 could be better.

Closer agreement in figure 13 between their calculated r_e^2 (the ☒ points) and their measured r_e^2 (the o points) involves a larger value of σ^2 for a fixed $\frac{n_e}{N}$. This may or may not increase the estimate of v_o^2 since they have neglected to include in σ^2 the initial variance of the cloud, which is not negligible and the contribution of molecular diffusion such as expressed in equation 4.3a. To illustrate how the inclusion of these other factors would reduce the estimate of v_o^2 obtained by Zimmerman and Champion consider the following. Rosenberg (1959) reports that cloud "Echo", has a diameter of 2 km at 1.75 seconds after burst and 1.2 km at .75 seconds after burst. Zimmerman and Champion report an initial radius of 600 m. If we accept their estimate of 1200 m as the diameter at the beginning of the diffusive growth, one estimate of their initial variance might be $(230m)^2 = 5.29 \times 10^4 m^2$. For a $\sigma_o^2 \sim 5 \times 10^4$, and a molecular diffusion coefficient equal to 10^3 cm^2/sec, then for the calculation of v_o^2 the total variance of 15×10^4 m^2 is reduced by $\sigma_o^2 + 2Kt = 7 \times 10^4$ m^2, from which we obtain $v_o^2 = 8m^2/sec^2$. If the beginning of the diffusive stage of cloud growth was after 1.75 seconds when the cloud was about 2 km in diameter, then a correspondingly higher σ_o, say, 300 meters, would give a value of v_o^2 equal to 4 m^2/sec^2.

These smaller estimates of v_o^2 are more consistent with those obtained from the sodium trails. In figure 10, if we evaluate the σ^2 curve in terms of $\sigma^2 = v_o^2 t^2$, the value 6 m^2/sec^2 is obtained for v_o^2; in figure 7 the value of v_o^2 obtained by the gradient log column density method was 8 γ m^2/sec; and in figure 9 the computed r_e^2 were based upon a v_o^2 of 2 and 4 m^2/sec^2 but the range of v_o^2 represented by the extreme sequences of measured r_e^2 in that figure is closer probably to 1 to 6 m^2/sec^2.

The order of magnitude of the turbulence parameter, v_o^2, is fairly well established by these initial analyses of sodium and cesium clouds. But, unless the question of optical effects (such as changes in exposure time or stop number) on the time dependent photographic growth of the cloud is considered with some care (and more quantitatively than we have done in this study), the real value of these vapor cloud experiments as a means of distinguishing the time dependent form of atmospheric dispersion will be vitiated by ad hoc assumptions about atmospheric dispersion processes.

VI. CONCLUSIONS

a) In photographic studies of a dispersive light-scattering cloud, insufficient attention to the details of image formation can lead to errors when interpreting image growth in terms of atmospheric turbulence.

b) Below 110 km and over a time interval of 700 to 800 seconds, the most probable interpretation of the horizontal accelerated expansion of sodium clouds is the relative dispersion law, $\sigma^2 \sim t^2$, in which the rate of change of standard deviation is about 2 m/sec.

c) The variability in the evidence for accelerated cloud expansion suggests that a $\sigma^2 \sim t^3$ dispersion law is as likely a $\sigma^2 \sim t$ law. The determination of the true dispersion law representing sodium cloud expansion requires the separation of atmospheric dispersion effects from the non-dispersive optical effects on image growth.

d) The results of the cloud exapnsion on 24 May 1960 and 17 September 1961 at heights of 108 to 109 km indicate that there is not a unique equivalence between the rate at which a cloud grows and its physical appearance, "irregular," "globular," or "smooth."

VII. RECOMMENDATIONS FOR FUTURE RESEARCH

1. Obtain a larger sample of dispersion statistics.

   a) Apply the maximum radius method, gradient ln n method, and (4.2) to cloud expansion data for the other morning and evening photographs which are available.

   b) Compare the results of the different analysis techniques on different film type from the same camera site (for the same cloud).

   c) Consider how to best determine σ^2 when the distribution of luminous intensity across the cloud image is non-Gaussian. Determine, if possible, under what conditions the other techniques for computing σ^2 (such as gradient ln n and 4.2) can still be used when the distribution of luminous intensity is non-Gaussian.

2. Design future vapor trails experiments to maximize the continuity of non-dispersive (optical) effects on image formation.

   a) Use films with overlapping regions of constant γ in separate cameras at the same site. (see insert)

   b) Unless the effects of stop changes on cloud growth can be made quantitative, maintain a constant aperture opening (f/stop) and a fixed exposure sequence (2-8-12 second exposure sequence every 30 seconds, for example)

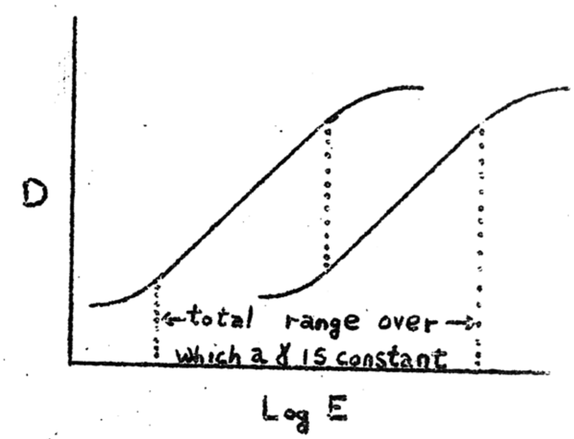

to eliminate abrupt changes in background density.

c) Various time intervals in the growth of cloud size (r_e^2) might be observed by adjusting the time of rocket launch with respect to solar depression angle so that the cloud image for longer diffusion times may be obtained. A better analysis of the Firefly data, with their larger initial size, should be performed.

d) Determine as accurately as possible the functional form of γ for all films used in these (twilight sky) diffusion studies.

3. In the event that film with a region of constant γ cannot cover all times of twilight photography, then attenuation effects of the natural sodium and ozone layers should be considered as a further non-dispersive effect on cloud image formation (and analysis), particularly when the incoming solar rays pass throught these layers at grazing incidence.

4. Puff-type experiments should be designed to compensate for the deficiencies of the trail experiments: they could be used below 95 km (the rate of chemical consumption could be treated as a variable) and they would not be subject to the image overlap of the trails (they must have a less energetic formation mechanism than the Firefly puffs).

- Note 1 -

One possible explanation would be suggested:

First, if two camera stop changes had been made, one between 220 and 250 seconds and the other between 340 seconds and 380 seconds,

Second, if the sky background intensity decreased enough between 220 seconds and 310 seconds to decrease the total magnitude of ln E, which determines the cloud edge, to the point where the magnitude of γ would decrease significantly with further decreases in sky beackground.

The decrease in γ would decrease the degree of contrast between cloud and sky (making definition of the visible diameter uncertain) until 340 seconds. At 340 seconds, the stop change (increase in aperture size allowing the film to subtend a greater solid angle for each point in the cloud) would hypothetically increase the ln E values defining the cloud edge back into the range where γ would again be constant and the contrast between cloud and sky would be maximized.

References

Batchelor, G.K., 1950: "Application of the Similarity Theory of Turbulence to Atmospheric Diffusion, " Quart. J. Roy. Meteor. Soc. 76, 133-146.

_______________, 1952: "Diffusion in a Field of Homogeneous Turbulence II. The Relative Motion of Particles," Proc. Cambridge Phil. Soc. 48, 345-363.

_______________, 1963: The Theory of Homogeneous Turbulence, Cambridge University Press, Cambridge, 197 pp (1959 Students' Edition).

Blamont, J.E. and Baguette, J.M., 1961: "Measures déduites des deformations de six nuages de metaux alcalins formés par fusées dans la haute atmosphere," Ann. de Geophys. 17, 319-337.

Blamont, J.E. and De Jager, C., 1961: "Upper Atmospheric Turbulence Near the 100 km Level," An. Geophys. 17, 134-144.

Bedinger, J.F., Manring, E.R. and Ghosh, S.N., 1958: "Study of Sodium Vapor Ejected into the Upper Atmosphere," J. Geophys, Res. 63, 19-29.

Chamberlain, J.W., 1961: Physics of the Aurora and Airglow, Academic Press, New York and London 704 pp.

Chapman, R., Dalgarno, A., Jones, R., and Beining, D., 1962: Investigation of Auroral, Airglow and Night Emissions As Related to Space-Based Defense Systems. Final Report. Volume 1. ARPA Order No. 237-61 Geophysics Corporation of America. 411 pp.

Chapman, S. and Cowling, T.G., 1939: The Mathematical Theory of Non-Uniform Gases, at The University Press, Cambridge, 245 pp.

Donahue, T.M. and Foderaro, A., 1955: "The Effect of Resonance Absorption on the determination of the height of the airglow layers," J. Geophys. Res. 60, 75-86.

Edwards, H.D., Cooksey, M.M., Justus, C.G., Fuller, R.N., Albritton, D.L., and Rosenberg, N.W., 1963: "Upper-Atmosphere Wind Measurements Determined from twelve Rocket Experiments," J. Geophys. Res. 68, 3021-3032.

Greenhow, J.S., 1959: "Eddy Diffusion and its Effect on Meteor Trails," J. Geophys. Res. 64, 2208-2209.

Korchigina, K.K., Myukhkyurya, V.I. and Smirnova, T.A. 1959: Raspred. Yarkosti po Dnevnomu i Nochnomu. Trudy, Glavnaya Geofizicheskaya Observatoriya Imeni A. I. Voyeykova Trudy No. 93,95-103.

Kraichnan, R.H., 1962: "The Closure Problem of Turbulence Theory" in Hydrodynamic Instability, Vol. 13, Proceedings of Symposia in Applied Mathematics, ed. G. Birkhoff, Amer. Math., Soc., Providence.

Lin, C.G., 1960: "On a Theory of Dispersion by Continuous Movements," I, Proc. Natl. Acad. Sci. 46(4), 566-570; II, Proc. Natl. Acad. Sci. 46(8), 1147-1150.

Manring, E.R., Bedinger, J.F. and Knaflich, H., 1961: "Some Measurements of Winds and the Coefficient of Diffusion in the Upper Atmosphere" in Space Research II ed. by van de Hulst, H.C., De Jager, C. and Moore, A.F., New York, Interscience Publishers, Inc., 1107-1124.

Manring, E.R. 1961: Detectability of Point Sources of Light and of Particulate Clouds in the Upper Atmosphere. (unpublished manuscript).

Manring, E.R. and Levy, R.J., 1961: "Photography of Luminous Extended Objects Against A Twilight Sky," Geophysics Corporation of America Tech. Rep. 61-4-N, contr. no. NAS5-215, March, 19 pp.

Minnaert, M., 1953: The photosphere, in The Sun (G.P. Kuiper, ed.) Chap. III, Univ. of Chicago Press, Chicago, 88-185.

Noel, T.M., 1963: "A Measurement of Turbulence Power and Small Eddy Scale Near 105 Kilometers," J. Geophys. Res. 68, 2862-2863.

__________, 1964: Private Communication.

Rees, J.A., 1961: "Diffusion Coefficients Determined From Sodium Vapor Trails," Planet. Space Sci. 8, 35-42.

Rosenberg, N.W., 1959: Project Firefly 1959, Part I Semi-annual Report ARPA 42-59, Geophys. Res. Dir. AFCRL, Bedford, Massachusetts.

__________, 1960: Project Firefly 1960, Volume I, Semi-annual Report under ARPA- order 42-60 and DASA MIPR 528-61, Geophys. Res. Dir. AFCRL, Bedford, Massachusetts.

Taylor, G.I., 1935: "Statistical Theory of Turbulence IV - Diffusion in a Turbulent Air Stream," Proc. Roy. Soc. Lond., Ser. A 151, 465-478.

Tchen, C.M., 1954: "Transport Processes as Foundations of the Heisenberg and Obukhov Theories of Turbulence, " Phys. Rev. 93(1), 4-14.

__________, 1961: Diffusion of Particles in Turbulent Flow," in Advance in Geophysics, number 6, Academic Press, New York 165-173.

Townsend, A.A. 1954: "The Diffusion Behind a Line Source in Homogeneous Turbulence," Proc. Roy. Soc. London 224, 487-512.

Zimmerman, S.P. and Champion, K.S.W., 1963: "Transport Processes in the Upper Atmosphere," J. Geophys. Res. 68(10), 3049-3056.